Dopamine transmission in the anterior insula shapes the neural coding of anxiety

Authors: Yoni Couderc[1], Tanmai Dhani Reddy[1], Giovanni Vardiero[1], Archi Garg[1], Daria Ricci[1], Marion d'Almeida[1], Céline Nicolas[1], Tina Habchi[1], Yue K. Wu[2], Julijana Gjorgjieva[2], Yulong Li[3], Emmanuel Valjent[4], Anna Beyeler[1]*

Affiliations

[1] Neurocentre Magendie, INSERM 1215, Université de Bordeaux, 146 rue Léo Saignat, 33000 Bordeaux, France

[2] School of Life Sciences, Technical University of Munich, Freising, Germany

[3] State Key Laboratory of Membrane Biology, Peking University School of Life Sciences, Peking-Tsinghua Center for Life Science, IDG/McGovern Institute for Brain Research at PKU, Beijing, China

[4] IGF, Université Montpellier, CNRS, INSERM, Montpellier 34094, France

*Correspondence to: Anna Beyeler (anna.beyeler@inserm.fr)

Abstract

The insular cortex (or insula), and particularly its anterior region, plays a crucial role in the control of emotional valence and anxiety (Etkin & Wager, 2007; Méndez-Ruette et al., 2019; Nicolas et al., 2023). While dopamine neurotransmission is known to modulate anxiety levels in humans (Hjorth et al., 2021) and animal models (de la Mora et al., 2010; Bananej et al., 2012; Zarrindast & Khakpai, 2015; DeGroot et al., 2020; Godino et al., 2023), its regulatory effects on the anterior insula remained unexplored. Here, using a multifaceted approach, we uncovered how dopamine shapes anterior insula function in anxiety and valence processing. First, we revealed a high density of neurons expressing type-1 dopamine receptors (D1) in the insula, particularly important in the anterior insula, and seven times greater than the density of neurons expressing type-2 dopamine receptors (D2). Few neurons co-expressed *Drd1 and Drd2* mRNAs in the anterior and posterior insula, and the density of *Drd1*+ neurons in the anterior insula was twice higher among inhibitory neurons than excitatory neurons. Second, we found that pharmacological activation of D1 in the anterior insula is anxiogenic, suggesting a direct link between insular dopamine signaling and anxiety-related behaviors. Using fiber-photometry recordings, we identified that the amplitude of dopamine release onto D1+ neurons in the anterior insula while mice were in anxiogenic spaces or receiving mild foot shocks was both positively correlated with mice level of trait anxiety. Population dynamics and deep-learning analyses of anterior insula single-unit recordings uncovered distinct coding patterns of anxiety-provoking and safe environments, as well as tastants of positive and negative valence. Remarkably, systemic D1 activation, which heightens anxiety-related behaviors, dampens this coding dichotomy by increasing coding variability for protected spaces while increasing the coding reliability for anxiogenic spaces. Interestingly, the coding reliability of anxiogenic areas was positively correlated with mice level of trait anxiety, and we observed a trend towards a positive correlation between the coding reliability of a negative tastants, and mice level of anxiety. Altogether, our findings provide a new model of neural population coding of anxiety and emotional valence and unravel D1-dependent coding mechanisms in the mouse anterior insula.

Main

Anxiety is an adaptive response to potential threats, yet persistently high levels of anxiety can become pathological (Belzung & Griebel, 2001; Daviu et al., 2019). Anxiety disorders are the most prevalent psychiatric conditions, characterized by chronic high levels of anxiety along with other symptoms, including an attentional bias towards negative valence. The insular cortex (IC or insula) has been implicated in both valence processing and anxiety disorders. Indeed, neuroimaging studies have shown overactivation of the insula in patients with anxiety disorders in response to salient and negative stimuli (Paulus & Stein, 2006; Shah et al., 2009; Etkin & Wager, 2007; Klumpp et al., 2013; Alvarez et al., 2015; MacLeod et al., 2019). Pharmacological and optogenetic studies in animal models have further demonstrated the anxiogenic properties of anterior insula (aIC) activation (Méndez-Ruette et al., 2019; Nicolas et al., 2023). While dopamine plays a crucial role in reward and motivation (Bromberg-Martin et al., 2010; Watabe-Uchida et al., 2017), it is also known to impact anxiety levels through its actions on D1-like and D2-like receptors (D1 and D2) in humans (Hjorth et al., 2021) and pre-clinical models (de la Mora et al., 2010; Bananej et al., 2012; Zarrindast & Khakpai, 2015; DeGroot et al., 2020; Godino et al., 2023; Tong et al., 2023). For example, photostimulation of D1+ neuron terminals of the medial prefrontal cortex (mPFC) within the basolateral amygdala (BLA) in mice was sufficient to induce rapid antidepressant and anxiolytic effects (Hare et al., 2019). In contrast, pharmacological activation of D1 in the BLA was shown to induce anxiogenic effects (Bananej et al., 2012), highlighting the complex and region-specific nature of dopaminergic regulation of anxiety. Despite the expression of D1 in the insula (Hurd et al., 2001), its role within this region in the regulation of anxiety remains unexplored. Using anatomo-functional, pharmacological and electrophysiological approaches, as well as advanced computational methods, we reveal how dopamine controls anterior insula functions through D1 activation, which concomitantly impacts anxiety-related behaviors.

Dopaminergic profile of the insular cortex

To characterize the dopaminergic innervation of the insular cortex, we employed retrograde tracing combined with tyrosine hydroxylase (TH) immunofluorescence. We injected retrograde tracers (CTB) in the anterior and posterior insular cortex (aIC and pIC, respectively) and imaged cell bodies in the ventral tegmental area (VTA) and substantia nigra pars compacta (SNc, Fig. 1a,b and Extended Data Fig. 1a). Neurons were classified as dopaminergic and projecting to the insula when co-labeled with TH staining and the retrograde tracer. These dopaminergic neurons predominantly innervate the aIC compared to the pIC (Fig. 1c). However, an anterograde viral strategy in a dopaminergic reporter line (DAT-cre) revealed similar dopaminergic axonal densities from VTA and SNc to both aIC and pIC (Extended Data Fig. 1b-e). To assess the distribution of neurons expressing D1 or D2, we used D1-cre and D2-cre mouse lines crossed with a reporter line (Ai14) to obtain double transgenic mice expressing tdTomato specifically in D1+ or D2+ neurons, respectively (Fig. 1d and Extended Data Fig. 1f). We observed a higher density of D1+ neurons in the aIC, compared to the pIC, which was seven times higher than the density of D2+ neurons in both aIC and pIC (Fig. 1e). Across cortical layers, D1+ neurons are denser in aIC layer 2/3, and are denser in the aIC compared to pIC within this layer (Fig. 1f). Conversely, D2+ neurons are

equally abundant in aIC and pIC (Fig. 1g and Extended Data Fig. 1g). D1+ neurons also represent a larger proportion of inhibitory compared to excitatory neurons, selectively in aIC (Fig. 1h). In contrast, D2+ neurons represent similar proportion of excitatory and inhibitory neurons in both aIC and pIC (Fig. 1i). Interestingly, long-range synaptic tracing of D1+ neurons of both aIC and pIC revealed that these neurons strongly project to amygdala nuclei and the contralateral insula (Extended Data Fig. 1h-l), as observed for glutamatergic insula neurons (Gehrlach et al., 2020; Nicolas et al., 2023; Glangetas et al., 2024).

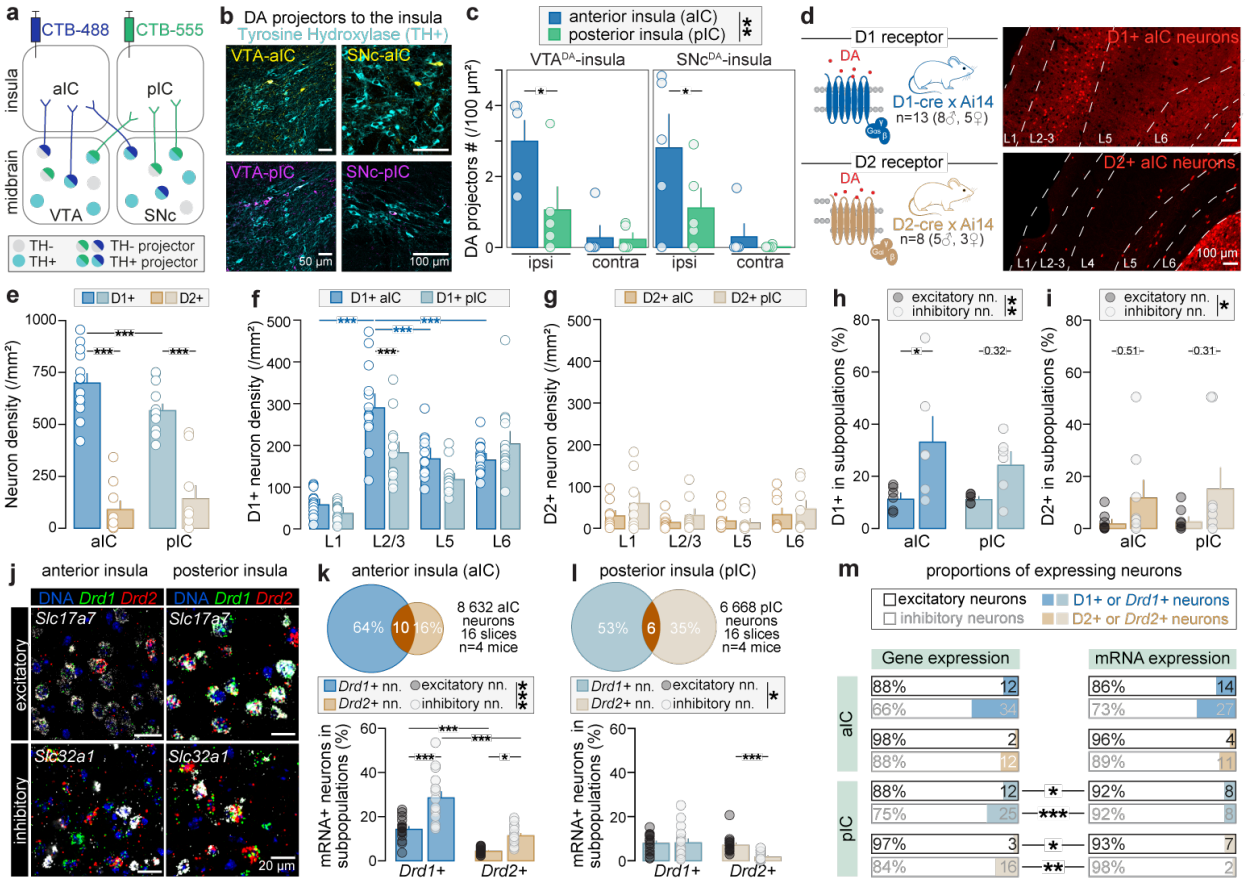

Fig. 1: Dopaminergic system in the insular cortex. a, Retrograde tracing strategy of neurons projecting to the anterior (aIC) and posterior (pIC) insular cortex, followed by immunohistochemical staining against tyrosine hydroxylase (TH) expressed in dopaminergic neurons. **b,** Confocal images showing two dopaminergic neurons targeting the insula from the VTA (left) and SNc (right). **c,** Number of VTA_{DA}-insula and SNc_{DA}-insula neurons located in the contralateral and ipsilateral side of the tracer injection (Region (aIC/pIC): $F_{(1,32)}$=7.94, **p=0.0082, Side (ipsi/contra): $F_{(3,32)}$=8.62, ***p=0.0002). **d,** Confocal images of tdTomato expression in D1+ and D2+ neurons across aIC cortical layers. **e,** Density of dopaminoceptive neurons in aIC and pIC showed a significant effect based on receptor type (D1+/D2+): $F_{(1,20)}$ = 87.9, ***p< 0.0001, with no significant effect of the Region ($F_{(1,20)}$=1.73, p=0.2039) but a significant interaction between Receptor type and Region ($F_{(1,20)}$=9.16, **p=0.0067) with more D1+ neurons than D2+ neurons in the aIC (***p<0.0001). **f,** Density of D1+ neurons across aIC and pIC cortical layers (Region: $F_{(1,48)}$=11.7, **p=0.0013, Layer: $F_{(1,48)}$=108, ***p<0.0001, interaction: $F_{(1,48)}$=6.93, *p=0.0114), higher in layer 2/3 of aIC compared to pIC (***p=0.0003). **g,** No difference in the density of D2+ neurons across aIC and pIC cortical layers (Region: $F_{(1,56)}$=3.13, p=0.0824, Layer: $F_{(3,56)}$=1.41, p=0.2494). **h,** Proportion

of D1+ neurons in excitatory and inhibitory subpopulations in aIC and pIC (Region: $F_{(1,20)}$=0.711, p=0.409, Subpopulation (excitatory/inhibitory): $F_{(1,20)}$=10.8, **p=0.0037). The proportion of D1+ neurons is greater in inhibitory neurons than excitatory neurons in aIC (*p=0.0412) but not pIC (p=0.33). **i,** Proportion of D2+ neurons in excitatory and inhibitory subpopulations in aIC and pIC (Region: $F_{(1,28)}$=0.169, p=0.6844, Subpopulation: $F_{(1,28)}$=4.99, *p=0.0337). **j,** Confocal images of *Drd1* and *Drd2* mRNA expression in excitatory (*Slc17a7*+, top) and inhibitory (*Slc32a1*+, bottom) neurons in aIC and pIC. **k,** Colocalization (8 632 aIC neurons, 16 slices, n=4 mice) and proportion of *Drd1*+ and *Drd2*+ mRNAs among excitatory and inhibitory neurons in aIC (Receptor (*Drd1*/*Drd2*): $F_{(1,60)}$=69.8, ***p<0.0001, Subpopulation: $F_{(1,60)}$=42.6, ***p<0.0001, interaction: $F_{(1,72)}$=4.89, *p=0.0308). **l,** Colocalization (6 668 pIC neurons, 16 slices, n=4 mice) and proportion of *Drd1*+ and *Drd2*+ mRNAs among excitatory and inhibitory neurons in pIC (Receptor: $F_{(1,60)}$=9.76, **p=0.0027, Subpopulation: $F_{(1,60)}$=4.70, *p=0.0341, interaction: $F_{(1,60)}$=5.9, *p=0.0182). **m,** Summary diagram of D1+ and D2+ neurons expression in the insula (two-tailed unpaired *t*-tests, *cf.* Table 2 for statistical values). **a-c**: aIC (n=5 mice) and pIC (n=5 mice). **d-i:** D1 (n=13 mice) and D2 (n=8 mice). **c, e-i, k-l**: Statistical analyses were conducted using a two-way ANOVA followed by Tukey's post-hoc tests. Data are presented as mean ± SEM.

To quantify the co-expression of dopamine receptors in the insula, we performed fluorescent *in situ* hybridization (FISH) for *Drd1* and *Drd2* transcripts in the aIC and pIC (Fig. 1j). Only 10% of cells in the aIC and 6% in the pIC co-expressed *Drd1* and *Drd2* (Fig. 1k-l). In the aIC, the proportion of neurons expressing *Drd1* or *Drd2* was higher in inhibitory than excitatory neurons (Fig. 1k). In contrast, in the pIC, the proportion of *Drd1*+ neurons was similar in excitatory and inhibitory subpopulations, and the proportion of *Drd2*+ neurons was even lower in inhibitory compared to excitatory neurons (Fig. 1l). Interestingly, the proportion of excitatory and inhibitory neurons expressing dopaminergic receptors, quantified at the genetic (reporter line) or mRNA (FISH) levels was consistent in the aIC but divergent in the pIC (Fig. 1m). Indeed, in the pIC, the proportions of D1+ or D2+ neurons were generally lower at the mRNA level compared to the genetic level in excitatory and inhibitory subpopulations, suggesting a partially transient expression of *Drd2* in the pIC during development (Fig. 1m). Together, these findings highlight a predominant dopaminergic targeting of the aIC, compared to pIC, with a larger proportion of D1+ compared to D2+ neurons.

Differential dopamine dynamics in aIC and pIC during anxiety and valence-related behaviors

To investigate the dynamics of dopamine release in the aIC and pIC during anxiety- and valence- related behaviors, we expressed the dopamine sensor dLight1.1 (Patriarchi et al., 2018), under the control of the pan-neuronal promoter hSyn (Fig. 2a). Dopaminergic activity increased specifically in the aIC, but not the pIC, when animals were in anxiogenic environments such as open arms of the elevated-plus maze (EPM), or the center of the open-field test (OFT, Fig. 2b-e). Notably, mice level of trait anxiety, estimated by the time mice spent in the OFT center, tends to negatively correlate with aIC dopaminergic signal intensity when mice are located in EPM open arms (Fig. 2f), and negatively correlates with aIC dopaminergic signal intensity when mice are in the OFT center (Fig. 2g). Importantly, these correlations were absent in the pIC (Extended Data Fig. 2b-d). To assess dopamine release during valence-related behaviors, we conducted photometry recordings during sucrose and quinine consumption (Extended Data Fig. 2e-f), as well

as during mild foot shocks used as an unavoidable negative stimulus (Fig. 2h-i). While no signal change was observed during sucrose or quinine consumption, we detected an increase in dopamine release at the onset of foot shocks, specifically in the aIC but not pIC (Fig. 2h-i). These results reveal that exploring anxiogenic spaces, and exposure to negative stimuli induce dopamine release, specifically in the aIC. Given the specificity of dopamine release in the aIC during anxiogenic and aversive states, we focused our subsequent analysis on this section of the insula.

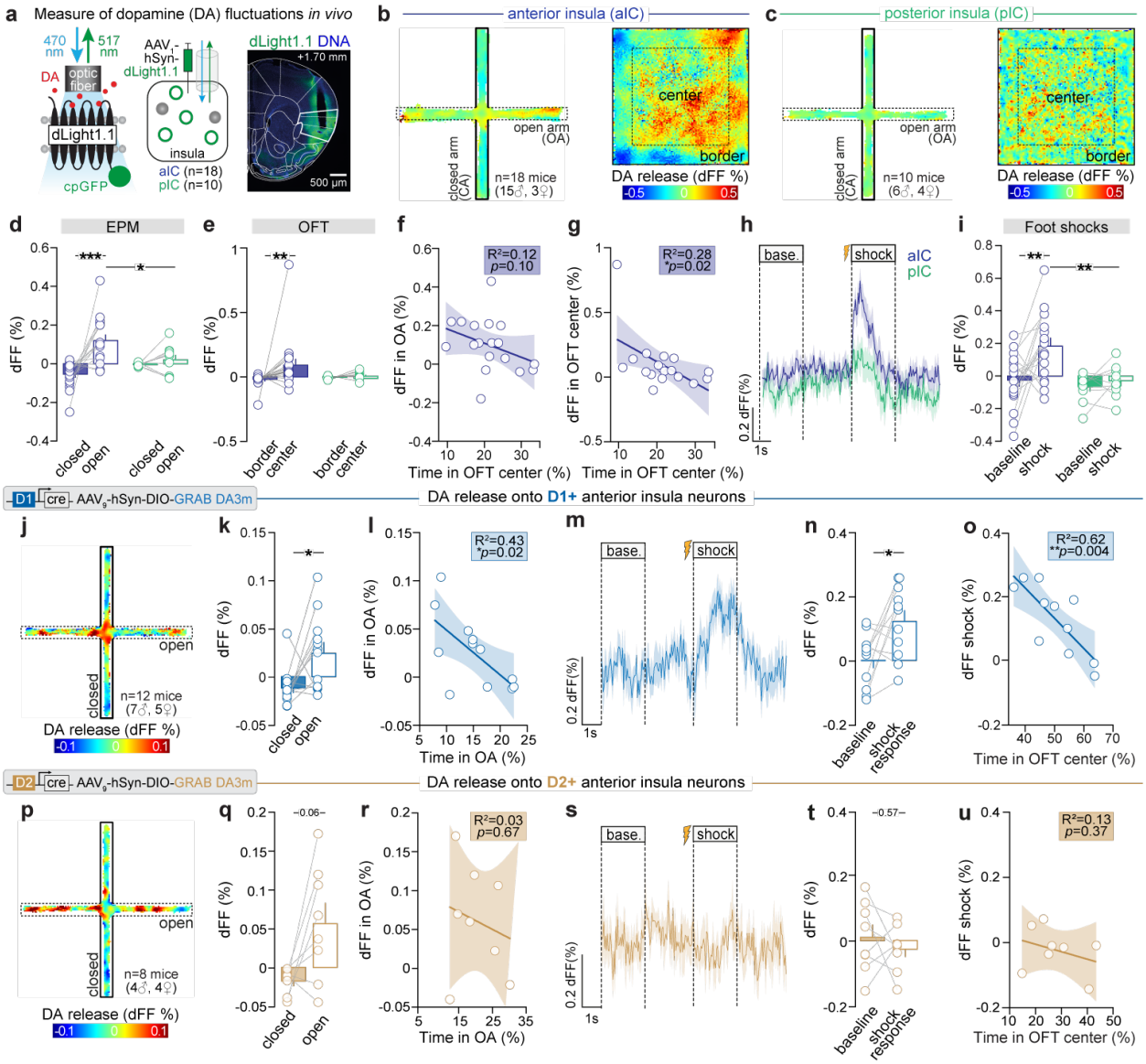

Fig. 2: Dopamine release in the insular cortex during anxiety- and valence-related behaviors. a, Viral strategy to express dLight1.1 to record dopamine (DA) release at the membrane of aIC or pIC neurons and histological verification after three weeks of expression. **b,** Averaged heatmap of DA release recorded in the aIC during the EPM (left) and OFT (right). dFF (%) represents fluorescent fluctuations from the mean level of the entire recording time series calculated over 60s around the sample. **c,** Averaged heatmap of DA release recorded in the pIC during the EPM (left) and the OFT (right). **d,** Averaged DA signal in aIC or pIC when mice are located in open and closed arms of the EPM (Arm: $F_{(1,52)}$=20.09, ***p<0.001, Region

(aIC/pIC): $F_{(1,52)}$=0.9755, p=0.3279, interaction: $F_{(1,52)}$=10.40, **p=0.0022). DA signal is higher when mice are in open compared to closed arms for aIC neurons (***p<0.001) and this increase is specific for aIC compared to pIC (*p=0.0221). **e,** Averaged DA signal in aIC and pIC when mice are in the center and borders of the OFT (Zone (border/center): $F_{(1,52)}$=5.538, *p=0.0224, Region (aIC/pIC): $F_{(1,52)}$=1.058, p=0.3085). DA signal is higher when mice are in the center compared to borders for aIC neurons (**p=0.0098). **f,** aIC DA signal when mice are in open arms tend to negatively correlate with the time mice spent in the OFT center (two-tailed Spearman correlation, R^2=0.1233, p=0.1041). **g,** aIC DA release when mice are in the OFT center negatively correlates with the time spent in the OFT center (two-tailed Pearson correlation, R^2=0.2773, *p=0.0248). **h,** Peri-shock time course of DA release in the aIC and pIC. **i,** DA release during foot shocks in the aIC and pIC compared to baseline (Period (baseline, shock): $F_{(1,52)}$=7.837, **p=0.0072, Region (aIC/pIC): $F_{(1,52)}$=8.45, **p=0.0054, interaction: $F_{(1,52)}$=4.049, *p=0.0494). DA release increases during foot shocks in the aIC (**p=0.0010) but not in the pIC (**p=0.0055). **j,** Averaged heatmap of DA release onto D1+ aIC neurons in the EPM. **k,** DA release onto D1+ aIC neurons is higher when mice are in open compared to closed arms of the EPM (two-tailed paired t-test, t=2.636, *p=0.0231). **l,** DA release onto D1+ aIC neurons when mice are in open arms negatively correlates with the time mice spent in open arms (two-tailed Pearson correlation, R^2=0.4339, *p=0.0198). **m,** Peri-shock time course of DA release onto D1+ aIC neurons. **n,** DA release during foot shocks onto D1+ aIC neurons compared to baseline (two-tailed unpaired t-test, t=2.790, *p=0.0191). **o,** DA release onto D1+ aIC neurons during foot shocks negatively correlates with the time mice spent in the OFT center (two-tailed Pearson correlation, R^2=0.62, **p=0.0039). **p,** Averaged heatmap of DA release onto D2+ aIC neurons in the EPM. **q,** DA release onto D2+ aIC neurons tends to be higher when mice are in open compared to closed arms in the EPM (two-tailed paired Wilcoxon test, p=0.0547). **r,** DA release onto D2+ aIC neurons when mice are in open arms does not correlate with the time mice spent in open arms (two-tailed Pearson correlation, R^2=0.03, p=0.6672). **s,** Peri-shock time course of DA release onto D2+ aIC neurons. **t,** DA release onto D2+ aIC neurons remains unchanged during foot shocks compared to baseline (two-tailed paired t-test, t=0.6025, p=0.5658). **u,** DA release onto D2+ aIC neurons during foot shocks does not correlate with the time mice spent in the OFT center (two-tailed Pearson correlation, R^2=0.13, p=0.3735). **d-e, i**: Statistical analysis were performed with two-way ANOVA and Tukey post-hoc tests. **a-i**: aIC (n=18 mice) and pIC (n=10 mice). **j-n:** aIC (n=12 mice). **o**: aIC (n=11 mice). **p-u**: aIC (n=8 mice). Data are presented as mean ± SEM.

To assess the specificity of dopamine release onto D1+ and D2+ neural subtypes during anxiety- and valence-related behaviors, we expressed the more sensitive dopamine indicator $GRAB_{DA3m}$ (Sun et al., 2020; Zhuo et al., 2024) selectively in D1+ or D2+ neurons of the aIC (Fig. 2j, Extended Data Fig. 2g-q). We observed increased dopamine release onto D1+ aIC neurons while mice were exploring EPM open arms (Fig. 2k) and OFT center (Extended Data Fig. 2i-n). Interestingly, the amplitude of this dopamine release when mice were in anxiogenic spaces, was negatively correlated with the total time mice spent in open arms, suggesting that mice with higher anxiety levels exhibit higher dopamine release onto D1+ aIC neurons when mice are in anxiogenic spaces (Fig. 2l, Extended Data Fig. 2i-m for OFT and Extended Data Fig. 11a-b). Importantly, these dopaminergic changes were not correlated with locomotor velocity in EPM open arms (Extended Data Fig. 2h). Regarding valence responses, we detected an increase in dopamine release onto D1+ aIC neurons at the onset of foot shocks compared to baseline levels (Fig. 2m-n), without changes during sucrose or quinine consumption (Extended Data Fig. 2o-p). The intensity of dopamine signal during foot shocks, positively correlated with mice levels of trait anxiety, estimated by the time spent in the OFT center (Fig. 2o). Dopamine release onto D2+ aIC neurons strongly tended to increase when mice explored EPM open arms and increased when mice were in the OFT center

(Fig. 2p-q and Extended Data Fig. 2r-w), but did not change at the onset of foot shocks (Fig. 2s-t). Importantly, none of the dopamine responses targeting D2+ neurons correlated with the total time mice spent in EPM open arms or OFT center (Fig. 2r, u and Extended Data Fig. 2u-x). Overall, these findings suggest a targeted increase of dopamine release within the aIC when mice explore anxiogenic areas, and are exposed to aversive stimuli, with a preferential D1-mediated response to negative valence.

D1 activation in the aIC promotes anxiety

Based on results presented beforehand and on the anxiogenic role of aIC (Méndez-Ruette et al., 2019; Nicolas et al., 2023), we evaluated whether systemic and intra-insular activation of D1R promotes anxiety in mice. First, we administered the selective D1 agonist SKF38393, or its Vehicle, intraperitoneally 30 minutes before behavioral testing (10 mg/kg, Fig. 3a). Notably, systemic activation of D1 resulted in a trend to reduce the time mice spent in EPM open arms, without altering locomotor activity (Fig. 3b-d). Second, to examine the specific impact of intra-aIC D1 activation on anxiety, mice were bilaterally implanted with cannulae and received local infusions of SKF38393 (0.25 mg/mL, Fig. 3e and Extended Data Fig. 3a) or its Vehicle. Remarkably, intra-aIC D1 activation decreased the time mice spent in open arms, while locomotor activity remained unaffected (Fig. 3f-g). Together, these findings indicate that D1R activation in the aIC induces anxiety-like behaviors, likely through anxiogenesis.

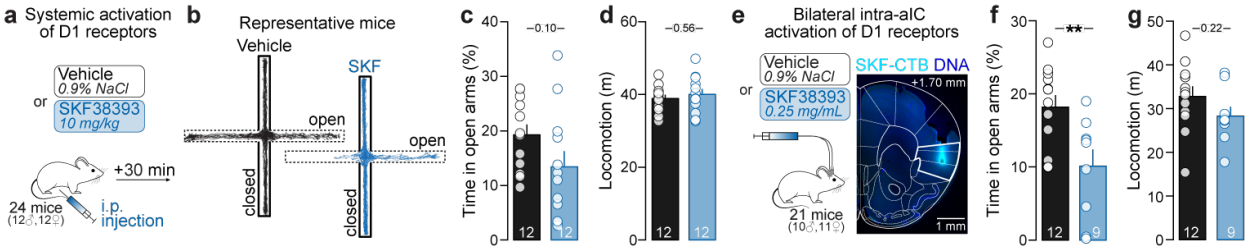

Fig. 3: Anxiogenic role of type-1 dopamine receptors (D1) in the aIC. a, Systemic activation of type-1 dopamine receptors (D1). Mice received an intraperitoneal (i.p.) injection of Vehicle or D1 agonist SKF38393 (SKF, 10 mg/kg) 30 minutes prior to the EPM test. **b,** Representative tracks of mice injected with Vehicle (left) or SKF (right). **c,** Mice who received SKF i.p. injection tend to spend less time in open arms compared to the Vehicle group (two-tailed unpaired *t*-test, t=1.699, p=0.1034). **d,** Total distance travelled in the EPM is similar between Vehicle and SKF mice (two-tailed unpaired *t*-test, t=0.5961, p=0.5572). **e,** Design and histological verification of intra-aIC D1 activation. Mice received a bilateral intra-aIC infusion of Vehicle or SKF38393 (SKF, 0.25 mg/mL) 6 minutes prior to the EPM test. Each injection was mixed with a fluorescent marker (CTB-AF488). **f,** Mice who received bilateral intra-aIC infusion of SKF spend less time in open arms compared to the Vehicle group (two-tailed unpaired *t*-test, t=2.972, $^{**}p$=0.0078). **g,** Total distance travelled in the EPM between Vehicle and SKF groups was not different (two-tailed unpaired *t*-test, t=1.281, p=0.2165). **a-d:** Vehicle (n=12 mice) and SKF (n=12 mice). **e-g:** Vehicle (n=12 mice) and SKF (n=9 mice). Data are presented as mean ± SEM.

Anxiety coding signature in the aIC

To decode the neural correlates of anxiety in aIC, we conducted *in vivo* extracellular recordings using 16-channel electrodes in mice freely exploring the EPM (Fig. 4a and Extended Data

Fig. 4a-b). We recorded 605 single units from 11 mice and analyzed their responses during three types of discrete behavioral events: entry into closed arms, entry into open arms, and head dips over the borders of open arms. Large proportions of units were excited at open arms entries (53%) and/or during head dips (57%), with a slightly lower proportion of units excited at closed arms entries (50%, Fig. 4b). Interestingly, the ratio of excited to inhibited units was higher for head dips (2.57), followed by open arm entry (1.80) and closed arm entry (1.68, Fig. 4b). We then analyzed the distribution of units in response to both open and closed arm entries (Fig. 4c). Strikingly, the largest class of units had opposite activities at open and closed arm entries (16% excited at closed and inhibited at open arm entries, and 15% inhibited at closed and excited at open arm entries), suggesting that about a third of aIC neurons encode anxiety-related information. The second largest proportion of units were excited at the entrance into both open and closed arms (28%), suggesting an involvement in coding salient events independently of their anxiogenic features.
To overpass the binary classification of units (excited or inhibited), we applied principal component analysis (PCA) to the single-unit data 6 seconds around each type of event (3 s before to 3 s after, Fig. 4d). PCA revealed gradually longer neural trajectories in the first three principal components (PCs) for more anxiogenic events. Indeed, the shortest neural trajectory was observed around closed arm entry, which was longer for open arm entries and longest during head dips (Fig. 4e), suggesting a more dynamic coding for anxiogenic environments. The longer the trajectory, the higher percentage of variance was explained by the three first PCs (Fig. 4f). However, support vector machine (SVM) decoding during the 6 seconds around salient events achieved only ~60% accuracy in distinguishing open and closed arms entries (Fig. 4g).

Thus, we utilized CEBRA (Schneider et al., 2023), a non-linear deep learning approach to integrate neural spiking over the entire recording (15 minutes, Fig. 4h). Remarkably, CEBRA uncovered latent structures of spiking reflecting the location of mice in anxiogenic and safe spaces, as distinct clusters of neural activity were associated with mice being located in open versus closed arms (Fig. 4i and Extended Data Fig. 5a). Moreover, k-Nearest Neighbor (kNN) decoding achieved above 80% accuracy in distinguishing open versus closed arms location, validating our CEBRA model (Fig. 4j). To further unravel how aIC encodes anxiety-related information, we computed the Shannon entropy of the open (OA) and closed arm (CA) latent clusters within each mouse embedding, used as a metric of the neural firing latent distribution when mice were located in OA or CA. Interestingly, Shannon entropy tends to be lower for the OA compared to the CA latent cluster (Fig. 4k), and OA latent cluster entropy was positively correlated with the time mice spent in open arms (Fig. 4l). This suggests a more defined coding for OA (smaller entropy) compared to CA in the aIC, and that more anxious mice have a more reproducible coding of open arms in the aIC.

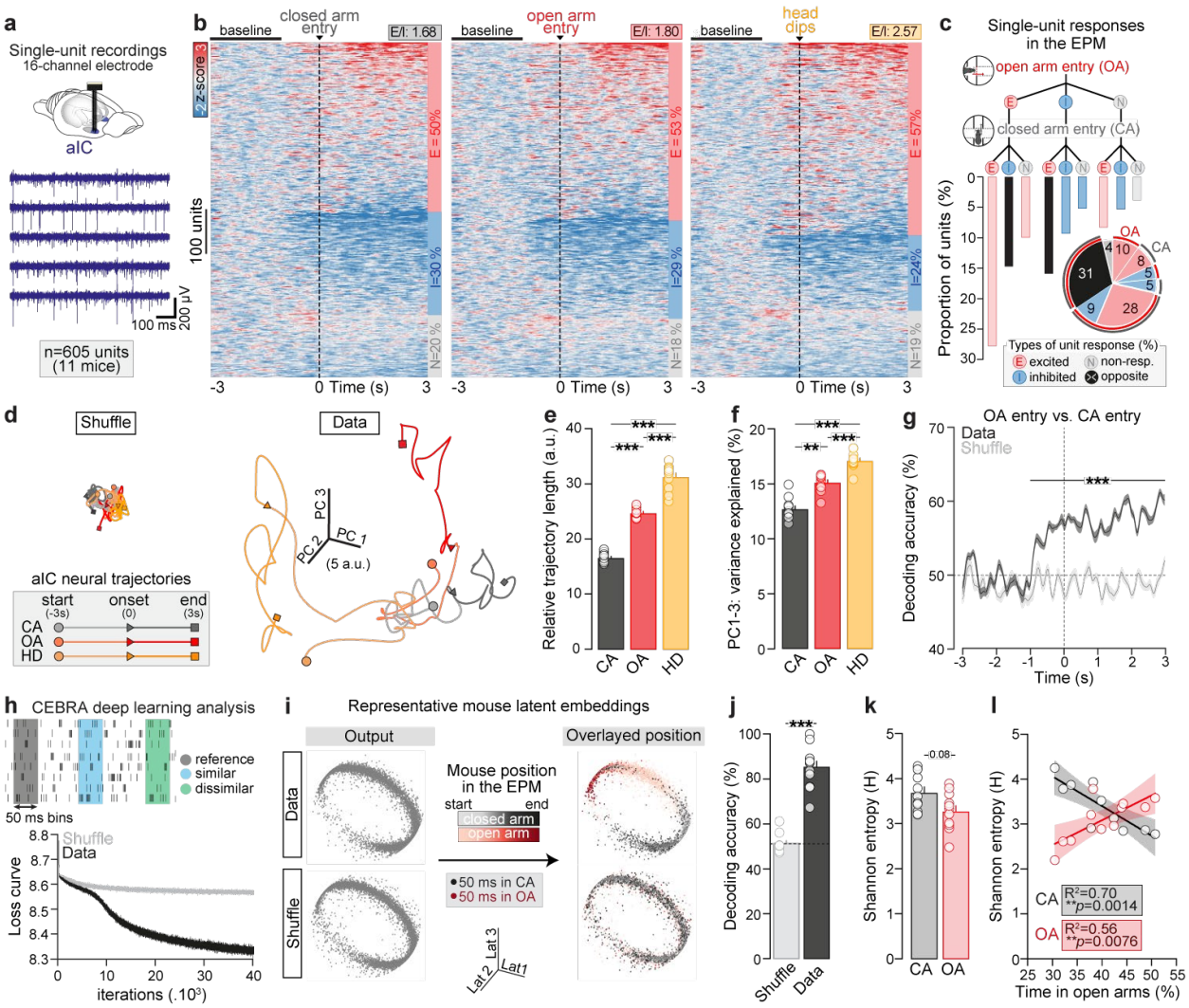

Fig. 4: Single-unit activity of aIC neurons in response to anxiogenic cues. a, Extracellular single-unit recordings in aIC using 16-channel electrodes with representative filtered traces (bottom). **b,** Heatmaps of *z*-scored peri-event firing activity when mice enter the closed arm (CA, left), open arm (OA, middle) or perform head dips (HD) in OA (right). Baseline window is -3 to - 1s. **c,** Proportion of units responding to OA and CA entry. First class of neurons has oppositive firing activity in OA and CA (31%) and the second class are both activated in OA and CA (28%). **d,** Principal component analysis (PCA) was applied on the firing pattern of all single aIC neurons recorded in response to three trial types: CA entry, OA entry and HD. Neural trajectories (Shuffle and Data) for the three trial types were projected onto the first three principal components explaining together 16,01 % of the variance (PC1=7.28 %, PC2=5.58 % and PC3=3.15 %). a.u.: arbitrary units. **e,** Relative neural trajectory lengths (Data-Shuffle) for the three event types ($F_{(2,30)}$=246.1, ***p<0.0001). Trajectory lengths were longer for OA entry (***p<0.0001) and HD (***p<0.0001) compared to CA entry. **f,** Variance explained by the first three principal components (PC) for the three trial types ($F_{(2,30)}$=72.06, ***p<0.0001), that is greater after OA entry (***p<0.0001) and HD (***p<0.0001) compared to CA entry. **g,** Support Vector Machine (SVM) was used to decode between two event types (CA entry and OA entry) using the neural activity of each event ($F_{(6,63)}$=281.4, ***p<0.0001). **h,** Deep learning neural analysis using CEBRA, a self-supervised nonlinear method for joint behavioral and neural embeddings, with a 50-ms binning (top) and loss curve validating our model as shown by the difference between Data and Shuffle (bottom). **i,** Representative CEBRA latent embeddings reveal differential coding of anxiogenic and safe spaces (n=1 mouse). Latent embeddings for Data and Shuffle

were plotted in the first three latent spaces and post hoc color coded based on the mouse position in the EPM (black: closed arms, red: open arms). **j,** a kNN (k-Nearest Neighbor) decoder achieved above 80% accuracy in distinguishing OA vs. CA entry, validating our CEBRA model (two-tailed paired *t*-test, t=13.06, ***p<0.0001). **k,** Shannon entropy of OA latent cluster tends to be lower compared to the CA cluster (two-tailed paired *t*-test, t=1.926, p=0.0829). **l**, Shannon entropy of the OA latent cluster correlates positively with the time mice spent in the OA (two-tailed Pearson correlation, R^2=0.5652, **p=0.0076) while the entropy of the CA latent cluster negatively correlates with the time mice spent in the OA (two-tailed Pearson correlation, R^2=0.6970, **p=0.0014). **e-g**: Statistical analysis were performed with one-way ANOVA and Tukey's post-hoc tests. **a-k**: aIC (605 units, n=11 mice). Data are presented as mean ± SEM.

Distinct encoding of positive and negative tastants by aIC neurons

To investigate the activity of individual aIC neurons in response to gustatory stimuli of positive and negative valence, we conducted extracellular recordings during random presentations of sucrose and quinine tastants (60 and 40% of trials, respectively, Fig. 5a). As expected, mice had a much higher licking rates for sucrose compared to quinine, confirming the aversive nature of quinine (Extended Data Fig. 6a-b). Among the 515 recorded aIC units, a slightly higher proportion of units were excited to quinine compared to sucrose (55% vs 52%), and the ratio of units excited compared to units inhibited (E/I) was higher during quinine consumption compared to sucrose consumption (2.50 vs 1.83, Fig. 5b). However, the averaged activity of single units excited to the tastant exhibited a greater amplitude in response to sucrose compared to quinine (Extended Data Fig. 6c). Interestingly, when examining responses to both sucrose and quinine, the largest group of neurons (35%) were excited by both stimuli, suggesting they encode salient events. The second group (19%) showed opposite responses, suggesting these neurons encode valence-related information.

Dimensionality reduction of population activity around the onset of licking bouts using PCA revealed a longer neural trajectory and a higher percentage of variance explained by the three first PCs for sucrose compared to quinine (Fig. 5d-f, Extended Data Fig. 6d-e), indicating differential encoding of positive and negative tastants. Finally, deep-learning CEBRA analysis uncovered distinct latent structures in aIC spiking during consumption of positive and negative tastants (Fig. 5h), and kNN clustering decoding achieved 70% accuracy in distinguishing sucrose and quinine trials (Fig. 5i, Extended Data Fig. 11c). Interestingly, while Shannon entropies for the sucrose and quinine latent clusters were not different, the entropy of the sucrose latent cluster tends to negatively correlate with the time mice spent in open arms (Extended Data Fig. 7b-c), indicating a less selective coding (higher entropy) for sucrose in the aIC as mice are more anxious. These findings demonstrate that aIC neurons differentially encode positive and negative taste valence at a population level.

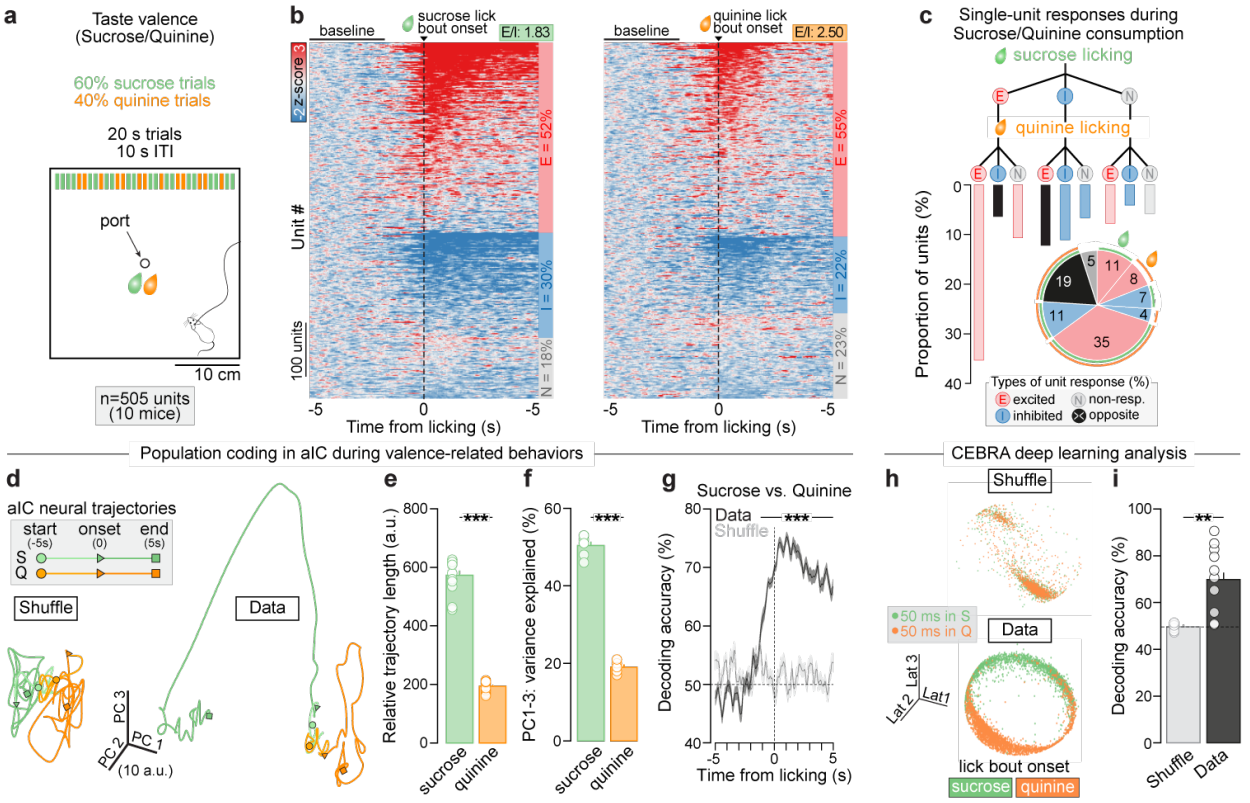

Fig. 5: Single-unit activity of aIC neurons in response to appetitive and aversive stimuli. a, Taste valence paradigm where mice consume sucrose and quinine. On 60% of trials sucrose was delivered (15% concentration, green), whereas on 40% of trials, quinine was delivered (1 mM, orange, 10 s inter-trial interval (ITI)). **b,** Averaged *z*-score peri-event firing after sucrose (left) and quinine (right) consumption, locked at the lick bout onset. **c,** Proportion of units responding to sucrose and quinine tastants. **d,** Principal component analysis (PCA) was applied on the firing pattern of all aIC single units recorded in response to sucrose and quinine consumption. Neural trajectories (Data and Shuffle) for trial types were projected onto the first three principal components explaining together 45,73% of the variance (PC1=31.82%, PC2=8.89% and PC3=5.02%). a.u.: arbitrary units. **e,** Relative neural trajectory lengths (Data-Shuffle) were longer for sucrose compared to quinine (two-tailed paired *t*-test, t=19.35, ***p<0.0001). **f,** Variance explained by the first three principal components (PC) is greater for sucrose compared to quinine (two-tailed paired *t*-test, t=33.64, ***p<0.0001). **g,** Support Vector Machine (SVM) was used to decode between sucrose and quinine event types using the neural activity of each event (one-way ANOVA, $F_{(5,49)}$=298.63, ***p<0.0001). **h,** Representative CEBRA latent embeddings reveal differential coding of appetitive and aversive stimuli (n=1 mouse). Latent embeddings for Data and Shuffle were plotted in the first three latent spaces and post hoc color coded based on the lick bout onsets (green: sucrose, orange: quinine). **i,** a kNN decoder achieved above 70% accuracy in distinguishing sucrose and quinine events, validating our CEBRA model (two-tailed paired *t*-test, t=4.622, **p=0.0013). **a-i**: aIC (505 units, n=10 mice). Data are presented as mean ± SEM.

Systemic activation of D1 disrupts the neural coding of anxiety in aIC neurons

To assess the causal impact of systemic activation of D1 on the neural coding of anxiety- and valence-related behaviors in the aIC, we conducted *in vivo* electrophysiology combined with systemic pharmacological activation of D1 (Fig. 6a and Extended Data Fig. 8a). Consistent with our findings (Fig. 3b), systemic D1 activation led to a reduction in the total time mice spent in

open arms compared to Vehicle-treated and non-injected controls (Fig. 6b and Extended Data Fig. 8b), underscoring the anxiogenic effect of D1 activation. Surprisingly, systemic D1 activation increased the proportion of units excited upon CA entry without altering the proportion of units excited upon OA entry, and even decreased the proportion of units excited during HD, compared to Vehicle (Fig. 6c). Interestingly, dimensionality reduction of population activity revealed altered neural trajectories following D1 activation. Specifically, the trajectory lengths were longer at CA entry and shorter around head dipping compared to Vehicle, suggesting a more defined coding for HD (Fig. 6d-e).

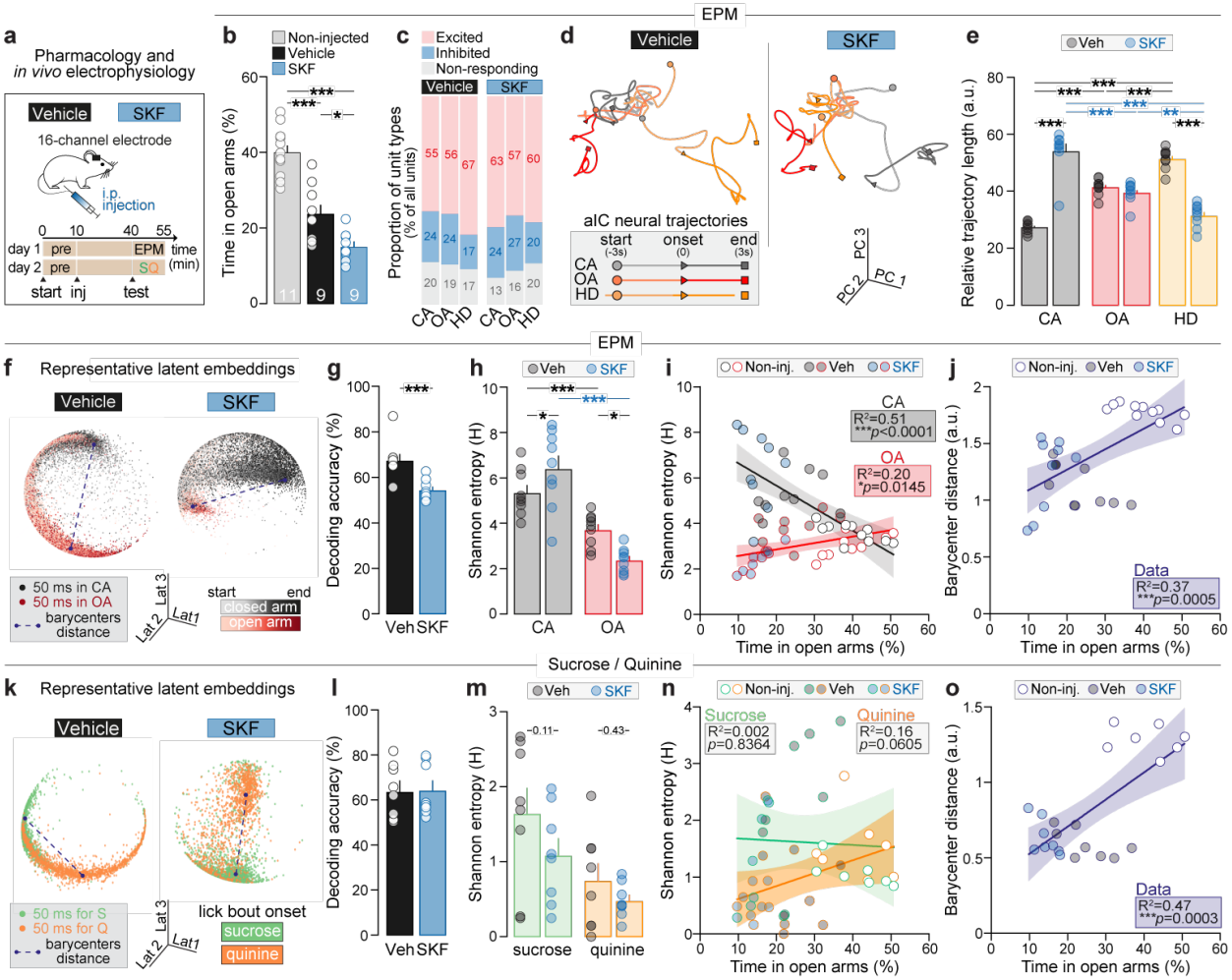

Fig. 6: Systemic activation of D1 receptors disrupts the population coding in aIC. a, Experimental timeline for pharmacology combined to *in vivo* electrophysiology. All mice were recorded during a 10 min baseline before Vehicle or D1 agonist SKF38393 (SKF, 10 mg/kg) was intraperitoneally (i.p.) injected, 30 minutes prior to the EPM test. **b,** Time spent in EPM open arms (one-way ANOVA, $F_{(2,26)}$=42.83, ***p<0.0001) is lesser for SKF-injected mice compared to the Vehicle-injected (*p=0.0152) and non-injected mice (***p<0.0001). **c,** Proportion of unit type activity in the closed (CA) and open (OA) arms under Vehicle and SKF conditions. **d,** Principal component analysis (PCA) was applied on the firing pattern of all aIC neurons recorded after Vehicle or SKF i.p. injections. Neural trajectories (Vehicle and SKF) for event types (CA entry, OA entry, HD) were projected onto the first three principal components explaining 17.37% (Vehicle) and 17.18% (SKF) of the total variance (Vehicle: PC1 = 7.83%, PC2 = 6.56% and PC3 = 2.98%; SKF: PC1 = 8%, PC2 = 5.89% and PC3 = 3.29%). a.u.: arbitrary units. **e,** Relative neural trajectory

lengths (Event (CA/OA/HD): $F_{(2,48)}$=0.198, p=0.8214, Condition (Vehicle/SKF): $F_{(2,48)}$=1.79, p=0.1868, Event x Condition interaction: $F_{(2,48)}$=135, ***p<0.0001) were longer for CA entry (***p<0.0001) and shorter for HD (***p<0.0001) after SKF compared to Vehicle. **f,** Representative CEBRA embeddings of 250-ms time bin spiking activity for Vehicle and SKF mice (n=2 mice). Latent embeddings were plotted in the first three latent spaces and post hoc color coded based on the mouse position in the EPM (black: closed arms, red: open arms). **g,** a kNN decoder achieved nearly 70% accuracy in differentiating OA from CA entries under the Vehicle condition, but accuracy remained at chance level following SKF injection (two-tailed paired t-test, t=4.201, ***p<0.0001). **h,** Shannon entropy (Arm (OA, CA): $F_{(1,16)}$=60.3, ***p<0.0001, Condition (Vehicle, SKF): $F_{(1,16)}$=0.152, p=0.7015, Arm x Condition interaction: $F_{(1,16)}$=10.8, **p=0.0046) was higher for the CA latent cluster (*p=0.0462) but shorter for the OA latent cluster (*p=0.0133) after SKF compared to Vehicle. **i,** Shannon entropy for the CA latent cluster negatively correlates with the time mice spent in open arms (two-tailed Pearson correlation, R^2=0.51, ***p<0.0001). Shannon entropy for the OA latent cluster positively correlates with the time mice spent in open arms (two-tailed Pearson correlation, R^2=0.20, *p=0.0145). **j,** Barycenter distance between OA and CA latent clusters positively correlates with the time mice spent in open arms (two-tailed Pearson correlation, R^2=0.37, ***p=0.0005). **k,** Representative CEBRA latent embeddings reveal a differential coding of appetitive and aversive stimuli after SKF injection (n=1 mouse), compared to Vehicle (n=1 mouse). Latent embeddings were plotted in the first three latent spaces and are post hoc color coded based on the lick bout onsets (green: sucrose, orange: quinine). **l,** Decoding accuracies remained at chance level following Vehicle and SKF injection (two-tailed unpaired t-test, t=0.086, p=0.9326). **m,** Shannon entropy (Tastant (Sucrose, Quinine): $F_{(1,28)}$=9.90, **p=0.0039, Condition (Vehicle, SKF): $F_{(1,28)}$=3.02, p=0.0931) tend to be lesser for sucrose latent cluster (p=0.1082) but remained unchanged for quinine (p=0.4309) after SKF compared to Vehicle. **n,** Shannon entropy for the quinine latent cluster tend to positively correlate with the time mice spent in open arms (two-tailed Pearson correlation, R^2=0.16, p=0.0605), while there is no correlation for the sucrose latent cluster (two-tailed Pearson correlation, R^2=0.002, p=0.8364). **o,** Barycenter distance between sucrose and quinine latent clusters positively correlates with the time mice spent in open arms (two-tailed Pearson correlation, R^2=0.4697, ***p=0.0003). **d, h, m**: Statistical analysis was performed with two-way ANOVA and Tukey post-hoc tests. **b-j**: EPM: Vehicle (397 units, n=9 mice) and SKF (309 units, n=9 mice). **k-o**: SQ: Vehicle (249 units, n=8 mice) and SKF (241 units, n=8 mice). Data are presented as mean ± SEM.

CEBRA deep learning analysis following systemic D1 activation revealed a qualitative increase of dispersion of the CA latent clusters (Fig. 6f and Extended Data Fig. 9a-b), associated with a decreased decoding accuracy in differentiating open and closed spaces (Fig. 6g). Consistently, after D1 activation, the Shannon entropy of the CA latent cluster increased compared to the Vehicle group, indicating a dispersion of neural activity during CA exploration (Fig. 6h). In contrast, the Shannon entropy decreased for the OA latent cluster following D1 activation, suggesting a more defined and selective neural activity of aIC neurons when mice are located in the OA (Fig. 6h). Notably, identical entropy values were obtained by analyzing an equal number of data points from open and closed arm clusters, confirming that the cluster dispersion of the closed arm activity after D1 activation is not merely a result of increased time spent in the closed arms (Extended Data Fig. 8e). Remarkably, when integrating the total time mice from all groups spent in open arms (11 non-injected, 9 Vehicle and 9 SKF38393), anxiety levels negatively correlate with Shannon entropy for OA latent cluster, while anxiety levels strongly and positively correlates with the entropy of the CA latent cluster. In other words, high-anxiety mice, which spend less time in open arms, show the lowest Shannon entropy for OA and the highest for CA. This indicates a more selective coding in the aIC neural population for OA and a more dispersed coding for CA as anxiety increases (Fig.

6i). Consistently with an increase in CA latent cluster dispersion, high-anxiety mice also exhibit a shorter distance between OA and CA latent cluster barycenters (Fig. 6j).

Systemic D1 activation alters the aIC neural structure of taste valence

Neural trajectory lengths for sucrose became shorter after systemic D1 activation, remaining unchanged for quinine (Extended Data Fig. 8h-i), suggesting a less dynamic coding for sucrose after D1 activation. Additionally, deep learning CEBRA analysis revealed qualitatively more dispersed sucrose and quinine latent clusters following D1 activation (Fig. 6k and Extended Data Fig. 10a-b). Although decoding accuracy remained unchanged (Fig. 6l), we observed a trend toward reduced Shannon entropy for sucrose following D1 activation, while the entropy for quinine was unaffected (Fig. 6m). Across the whole population of mice, we observed a trend of negative correlation between the entropy of the quinine cluster and the time mice spent in open arms (Fig. 6p). This indicates that high-anxiety mice show a trend for a reduced entropy of the quinine latent cluster, suggesting a more selective coding in the aIC for quinine when mice are more anxious (Fig. 6n, Extended Data Fig. 11d). Additionally, the barycenter distance between sucrose and quinine was reduced in high-anxiety mice (Fig. 6o). In summary, systemic D1 activation increases anxiety-related behaviors in the EPM and disrupts the representation of both anxiety-related environments and taste valence in the aIC.

Discussion

While dopamine neurotransmission is known to modulate anxiety levels in humans and animal models, its regulatory effects on the anterior insula remained unexplored. Here, we identified a higher density of D1+ compared to D2+ neurons throughout the insula, as well as a higher D1+ neuron density in the anterior part of the insula. We then revealed a selective increase of dopamine release in the anterior insula during the exploration of anxiogenic environments, and during exposition to aversive stimuli, the latter preferentially targeting D1+ neurons. Finally, using a combination of pharmacological manipulation, *in vivo* electrophysiology, and advanced computational tools, we revealed that systemic activation of D1 concomitantly heightens anxiety-related behaviors and disrupts neural coding of anxiety and taste valence in the anterior insula.

Dopaminoceptive profile of insula neurons

Using retrograde tracing, we found that dopaminergic neurons from the ventral tegmental area (VTA^{DA}) and substantia nigra pars compacta (SNc^{DA}) innervate preferentially the anterior compared to the posterior insula, consistent with previous findings (Ohara et al., 2003). Interestingly, anterograde tracing revealed similar overall densities of dopaminergic terminals in both the anterior and posterior insula, suggesting that dopaminergic neurons projecting to the posterior insula have denser axonal arborization as they are less numerous. Additionally, it has been established that VTA^{DA} neurons primarily innervate the inner layers of the insula, while SNc^{DA} neurons predominantly target superficial layers (Fallon, 1981).

Interestingly, D1+ neurons are denser in the anterior compared to the posterior insula, and they outnumber D2+ neurons, consistent with findings in other cortical regions (Meador-Woodruff et al., 1996). However, D1+ neurons primary location in layer 2/3 of the anterior insula contrasts with their arrangement in the medial prefrontal cortex (mPFC), where they are more numerous in deeper layers (Gaspar et al., 1995; Anastasiades et al., 2019). This suggests that D1+ neurons may serve a specialized function in the anterior insula. We further observed a higher proportion of D1+ neurons among inhibitory neurons than excitatory neurons in the anterior insula, evident at both genetic (reporter line) and mRNA levels (FISH). Conversely, in the posterior insula, D1+ neurons have similar proportions among inhibitory and excitatory neurons at both genetic and mRNA levels. These findings suggest the existence of a D1-mediated inhibitory microcircuit specific to the anterior insula. Notably, in the anterior insula, the proportion of labeled neurons from the reporter line (gene expression) and FISH were consistent, while they diverged in the posterior insula. Indeed, in the posterior insula, proportions were overall lower at the mRNA level, and *Drd2*+ neuron density was even lower among inhibitory compared to excitatory neurons. One interpretation of this discrepancy between genetic and mRNA measures could be that *Drd2* is mainly expressed during developmental and/or early-life stages (Wu et al., 2012; Herring et al., 2022). Finally, the sparse colocalization of *Drd1* and *Drd2* in the insular cortex emphasizes their distinct functional roles in this region as described for the prefrontal cortex (Jenni et al., 2017; Xing et al., 2022) or striatum (Gerfen et al., 1990; Bruce et al., 2024).

Selective dopaminergic control of anxiety in the anterior compared to posterior insula

Several studies have highlighted a functionally different role of the anterior and posterior insular cortex in anxiety-related behaviors. Indeed, pharmacological activation of the anterior insula increased anxiety levels in the elevated-plus maze, while pharmacological activation of the posterior insula decreased anxiety levels in rats (Méndez-Ruette et al., 2019). Additionally, we recently showed that pharmacological inhibition of the anterior insula in mice is anxiolytic (Nicolas et al., 2023), highlighting that the anterior insula processes and regulates anxiety bidirectionally. In the posterior insula, contrasting with pharmacological activations in rats (Méndez-Ruette et al., 2019), optogenetic activation of glutamatergic neurons in mice increased anxiety-related behaviors (Gehrlach et al., 2019).

Remarkably, the activity of anterior but not posterior insula excitatory neurons selectively increased when mice explored anxiogenic spaces, supporting a selective coding of anxiogenic environments in the anterior insula (Nicolas et al., 2023). Nonetheless, single-unit recordings identified the posterior insula as a key mediator of bottom-up cardiac interoceptive processing involved in anxiety. Notably, optogenetic inhibition of the posterior insula reduced anxiety-like behaviors induced by optical cardiac pacing (Hsueh et al., 2023; Couderc & Beyeler, 2023).

Dysfunction of dopaminergic pathways has been associated with trait anxiety as well as anxiety disorders (Zweifel et al., 2011; Morel et al., 2022; Zalachoras et al., 2022). Here, we uncovered a specific increase of dopamine release in the anterior but not the posterior insular cortex in response to an anxiety-provoking environment, as observed in the ventral hippocampus (Godino et al.,

2023) or interpeduncular nucleus (Molas et al., 2023). Strikingly, the amplitude of dopamine release in the anterior, but not the posterior insula, while mice were in anxiogenic spaces (EPM open arms and OFT center), was positively correlated with mice level of anxiety. This highlights a higher release of dopamine in the anterior insula while mice are located in anxiogenic spaces, as mice have a higher level of anxiety. Moreover, we also found a selective dopamine release in the anterior upon exposure to mild foot shocks. This suggests that dopamine release also regulates the processing of negative valence stimuli in the anterior insula, as described in the medial prefrontal cortex (mPFC) using fast-scan cyclic voltammetry (Vander Weele et al., 2018).

Differential dopamine release onto D1+ and D2+ anterior insula neurons

Notably, while dopamine release increased onto both D1+ and D2+ insula neurons when mice were located in exposed areas, we identified a specific increase of dopamine release onto D1+ neurons in response to aversive stimuli. Consistent with an implication of anterior insula D1+ neurons in negative valence, another recent study demonstrated that D1-like receptor activity in the insula increased the salience of stimuli, enabling the consolidation of aversive memories (Gil-Lievana et al., 2022). The selective dopamine release we observed onto D1+ neurons upon aversive stimuli could be explained by the higher density of D1+ compared to D2+ neurons across the insula or by the fact that dopamine has a 10 to 100 higher affinity for D2 than D1 (Martel & Gatti McArthur, 2020; Sippy & Tritsch, 2023). This affinity gap could dampen the signal detected from D2+ neurons, as the dopamine sensor used ($GRAB_{DA3m}$) is D1-based (Sun et al., 2020; Zhuo et al., 2024). However, these are both unlikely as the signal intensity recorded in the EPM and OFT is similar for D1+ and D2+ subpopulations. Yet, differential dopaminergic inputs to cortical layers in the insula could contribute to this D1+ neural population's selective dopaminergic signal upon exposure to aversive stimuli. Indeed, as D1+ neurons have a higher density in L2/3, a higher density of dopaminergic terminals in L2/3 could explain these differences.

Importantly, only the amplitude of dopamine release onto D1+ anterior insula neurons while mice were in anxiogenic spaces or receiving mild foot shocks was positively correlated with mice level of anxiety. These population-specific correlations between dopamine release and anxiety levels suggest that dopamine release onto D1+ neurons of the anterior insula selectively contributes to the control of trait anxiety in mice.

Single-unit response to anxiety and valence in the anterior insula

When analyzing the spiking activity at specific behavioral time points (entrance to anxiogenic and protected areas), about a third of neurons (31%) exhibited opposite responses at the entrance into exposed (open arms) and safe (closed arms) spaces, indicating they may encode anxiety-related information. In comparison, a slightly smaller subset of neurons (28%) was activated at the entrance of both protected and exposed areas and might, therefore, primarily encode salient events and/or arousal. In line with our findings, a recent study showed that the anterior insula is involved in stress-induced anxiety. Indeed, single-unit recordings of putative principal anterior insula

neurons revealed that around 27% of neurons were activated in response to a stressor, and this activity positively correlated with stress-induced defensive behaviors in mice (Park et al., 2022). Regarding taste valence, we observed that 35% of neurons were activated by both positive and negative tastant consumption, suggesting they encode salient events. In this case, only ~20% of neurons displayed opposite responses to positive and negative tastants, suggesting a fifth of neurons encode taste valence. Interestingly, we found a higher excitation-to-inhibition ratio in response to quinine consumption, reflecting a bias towards neural excitation in response to negative valence compared to positive valence.

Prior studies have investigated insula neuron coding properties in taste processing. Single-unit recordings in the insula revealed that around 46% of neurons changed their firing rates in response to food consumption in mice (Kusumoto-Yoshida et al., 2015; Livneh et al., 2017). Moreover, single anterior insula neurons recorded from Rhesus monkeys showed changes in activity during rewarded compared to unrewarded trials (Mizuhiki et al., 2007). In addition, recordings of calcium activity in individual intermediate insula neurons revealed that a large majority of neurons (around 80%) respond to water reward consumption (Livneh et al., 2020). These studies, among others (Peng et al., 2015; Vincis et al., 2020; Chen et al., 2021), which examined the canonical role of the anterior insular cortex in taste processing, confirmed its involvement in encoding both positive and negative tastes, which aligns with our current findings, further linking insular activity to valence processing.

Non-linear dimensionality reduction of neural activity

Conventional dimensionality reduction methods, such as principal component analysis (PCA), allow identifying low-dimensional patterns within high-dimensional datasets using linear transformations (Churchland et al., 2010; Cunningham & Yu, 2014; Pang et al., 2016). While this approach has been proven extremely valuable to dissecting population coding of cue-based behavioral analysis, it remains limited to integrating longer timescale activity, such as during anxiety or social behaviors, which last over minutes up to hours. Thus, linear dimensionality reduction techniques often fail to capture the structure of the whole data, as highlighted by the relatively low percentage of variance explained in our single-unit data during the elevated-plus maze exploration. Thus, we used a cutting-edge non-linear deep-learning approach, CEBRA (Consistent EmBedding of high-dimensional Recordings using Auxiliary variables, Schneider et al., 2023), which reduces the dimensionality of neuronal activity across the whole recording to discover latent features in time series data (Mathis et al., 2024). This innovative approach allowed us to uncover a differential coding of safe and exposed areas, as well as a differential coding of rewarding and aversive tastants in the anterior insula. Interestingly, a recent study used CEBRA to jointly analyze calcium activity from neural ensembles of the extended amygdala, with various behaviors, including exploration of anxiogenic spaces or quinine consumption (Chang et al., 2024). In that study, authors included both neural and behavioral data as CEBRA inputs and revealed an overlap between neural ensembles that are active when mice are in exposed areas or consuming quinine. Here, we leveraged CEBRA deep-learning algorithm with only neural data as

inputs (no behavioral data) which disentangled neural structures encoding anxiogenic and safe spaces over the entire recording, as well as neural structures encoding taste valence during the consumption of both positive and negative tastants, within the complex neural population dynamics. This powerful approach paves the way to crack neural structures of behaviors, which could be extended beyond anxiety and valence processing to explore other paradigms such as freely-moving social interactions (Bordes et al., 2023) or reward-motivated behaviors (Nicolas et al., 2019).

D1-mediated dopaminergic modulation of anxiety in the anterior insula

The dopaminergic system is crucial in filtering and prioritizing sensory information based on behavioral context and goals (Kim et al., 2020; Siju et al., 2020). In rodents, dopamine has been shown to modulate subcortical responses to unexpected auditory stimuli, highlighting its role in attention and novelty detection (Valdés-Baizabal et al., 2020). Similarly, dopamine-driven filtering mechanisms in Drosophila reduce threat perception as courtship progresses (Cazalé-Debat et al., 2024). Interestingly, a study in monkeys has shown that inhibiting D1 receptors in the lateral prefrontal cortex impairs the learning of novel associations while having little effect on familiar task performance. This suggests that D1 receptors are more critical for acquiring new information and adapting to new situations than for maintaining established behaviors (Puig & Miller, 2012). In our study, we show that both systemic and intra-anterior insula activation of D1 heightened trait anxiety levels, suggesting that anxiogenesis induced by systemic D1 activation is driven, at least partially, by D1 activation within the anterior insula. Following systemic D1 activation, we identified a striking alteration of neural coding, characterized by a more dynamic coding at the entrance of protected areas and less dynamic coding of head dips. Consistently, we also found a more dispersed neural representation (higher entropy) when mice are located in protected zones (closed arms) and a less variable representation (lower entropy) when mice are in anxiogenic spaces (open arms). This shift in coding was associated with a decreased distance between open and closed arm latent clusters. Interestingly, the nearer open and closed arm latent clusters were (low barycenter distance), the more anxious mice were. These findings suggest that D1 systemic activation disrupts the distinction between anxiogenic and safe spaces, potentially inducing a convergence of neural representations of safe and dangerous environments. Thus, by disrupting the encoding of anxious and safe environments, D1 activation could cause a brain state where mice could perceive safe areas as threatening.

While we cannot rule out the possibility that some of the effects on neural coding following D1 systemic activation may be mediated by D1 activation outside the insula, it is reasonable to infer that local D1 activation in the anterior insula contributes to these effects. To date, no study has investigated the impact of local nor systemic D1 activation on neural coding in other cortical or subcortical areas. In future experiments, we will investigate the direct impact of D1 within the anterior insula on anxiety by locally activating D1 in the anterior insula while recording single-unit activity in this region. However, our current work already provides a new perspective on how D1 activation shapes the neural coding of anxiety and valence.

Neural code linking emotional valence and anxiety in the anterior insular cortex

Several studies identified that highly anxious individuals show behavioral, cognitive, and neurophysiological alterations, including in valence processing (Weger & Sandi, 2018; Daviu et al., 2019; Nicolas et al., 2023). We recently demonstrated that the activity of excitatory neurons in the anterior insula when mice are exposed to negative stimuli is proportional to mice level of trait anxiety (Nicolas et al., 2023). Here, we identified a specific increase of dopamine release onto D1+ neurons in response to aversive stimuli. Importantly, the amplitude of this dopamine release was positively correlated with mice level of anxiety, suggesting that D1+ neurons of the anterior insula selectively contribute to the coding of negative valence stimuli. Similarly, following D1 activation, we found that the Shannon entropy of the quinine latent cluster tends to positively correlate with trait anxiety in mice, whereas no correlation was observed with positive valence. Our previous and current results pinpoint the anterior insula as a common substrate for both trait anxiety and negative valence and reveal that dopamine release in the anterior insula could contribute to this link through the activation of D1-expressing neurons. Moreover, the correlation between dopaminergic neural responses to negative valence (quinine consumption) and trait anxiety in mice further supports the idea that circuits encoding emotional valence may become maladaptive in anxiety disorders (Daviu et al., 2019; Lammel et al., 2014; Pignatelli & Beyeler, 2019).

Integrating circuits into the dopaminergic modulation of the anterior insula

Circuit dissection studies have provided essential knowledge about the contribution of neural circuits to anxiety and valence-related behaviors. Our anatomical results show that the projection pattern of D1+ excitatory neurons in the anterior and posterior insula mirrors those of all glutamatergic neurons. Given that the BLA is one of the primary output regions of the anterior insula and that we recently showed that anterior insula neurons projecting to the BLA (aIC-BLA) control anxiety (Nicolas et al., 2023), we hypothesize that D1-expressing neurons in the anterior insula projecting to the BLA (aIC^{D1}-BLA) selectively encode anxiety and negative valence. Indeed, our results suggest that adding dopaminergic molecular features to the definition of neural circuits would open new doors to identify unique neural populations controlling anxiety and/or emotional valence. An inspiring study recently combined projection and dopaminergic profiling to study social behaviors and recorded single-neuron calcium signals in D1+ anterior insula neurons projecting to the nucleus accumbens (aIC^{D1}-NAc) of freely moving mice. They revealed increased activity of aIC^{D1}-NAc neurons during positive and negative social interactions and identified social valence-dependent synaptic plasticity (Espinosa et al., 2024), emphasizing D1 as a key regulator of valence in the mouse insular cortex. Future research will explore the role of specific projection-defined D1+ subpopulations of the insular cortex in state and trait anxiety.

Conclusion

All in all, our findings provide the first evidence of a D1-mediated control of anxiety through neuromodulation of the anterior insular cortex. Our work also lays out an innovative approach using non-linear deep learning methods to dissect neural population dynamics underlying anxiety. In the long term, our work will serve as a starting point to understand how dopaminergic modulation of insular circuits contributes to anxiety disorders.

Material and methods

Animals and housing conditions. Male and female adult wild-type C57Bl/6J, D1-cre, D2-cre, D1-cre and D2-cre crossed with the Ai14 reporter and DAT-cre mice were at least 10 weeks old before being used for experiments. Animals were housed in controlled conditions of temperature and humidity environment, on a reversed 12h light/dark cycle and with *ad libitum* access to food and water. Animal maintenance, treatments and experimental procedures were conducted according to French governmental regulations and approved by the ethical committee and the Ministry of Education, Research and Innovation (APAFIS #30247) in accordance with the guidelines of the European Communities Council Directives.

Stereotaxic surgeries. Prior to surgery, animals were injected with Metacam (5 mg/kg), and all surgeries were conducted under aseptic conditions. Mice were anesthetized with isoflurane (5% induction, 1.5%-2.0% maintenance) in the stereotaxic frame and their body temperature was maintained with a heating pad. Health and weight checks were followed for three days post-surgery. Retrograde tracers or viral vectors were delivered via intracranial injections using glass micropipettes (3-000-203-G/X, Drummond Scientific) pulled with a puller (PC-100, Narishige) at a rate of 1 $nL.s^{-1}$ using a Nanoliter (Nanoliter2020, WPI). After completion of the injection, the pipette was left for an additional 5 min to allow diffusion of the tracer or the virus at the injection site and then slowly withdrawn before the skin incision was sutured. After surgery, the mouse's body temperature was maintained using a heat lamp until it fully recovered from anesthesia. Mice returned to their home cages for 1 week to allow retrograde tracer transport or 3 to 4 weeks to allow viral expression.

For anatomical characterization of dopaminergic inputs to the insular cortex (Fig. 1 and Extended Data Fig. 1), two strategies were used. In the first approach, Cholera toxin subunit B (CTB) coupled to AF488 or AF555 were injected in the aIC or pIC (counterbalanced). In the second approach, a cre-dependent adeno-associated of serotype 9 viral vector carrying the gene coding for a yellow fluorescent protein (AAV_9-EF1α-DIO-eYFP) was injected in the ventral tegmental area (VTA) and substantia nigra pars compacta (SNc) in different mice.

For the quantification of synaptic contacts of the D1+ insula neurons (Extended Data Fig.1), we injected a 1:2 mix of the cre-dependent viral vector expressing the enhanced yellow fluorescent protein eYFP (AAV_9-EF1α-DIO-eYFP) and an adeno-associated virus serotype 8/2 carrying the gene coding for the synaptophysin fused to the red fluorescent protein mCherry in a double-floxed inverted open reading frame (DIO) under the control of elongation factor 1a

promoter ($AAV_{8/2}$-EF1α-DIO-Synaptophysin-mCherry) in the aIC and pIC of D1-cre mice (aIC: n=5, pIC: n=6).

For fiber-photometry recordings of dopamine release (Fig. 2 and Extended Data Fig. 2), an AAV_1 carrying the dopamine sensor dLight1.1 (Patriarchi et al., 2018) gene under the hSyn promoter (AAV_1-hSyn-dLight1.1) was injected in the aIC and pIC, or an AAV_9 carrying the cre-inducible dopamine sensor $GRAB_{DA3m}$ (Sun et al., 2020; Zhuo et al., 2024) gene under the hSyn promoter (AAV_9-hSyn-DIO-$GRAB_{DA3m}$) was injected in the aIC of D1-cre (n=12) and D2-cre mice (n=8). An optical fiber was implanted after viral injections. An optical fiber (400 µm diameter, >90% efficiency, 0.39 numerical aperture (NA)) inserted in a 1.25 mm metal ferrule was implanted 50 µm above the viral vector injection site. Biocompatible cement and resin were used to keep the implanted fiber fixed in the brain. Mice returned to their home cages for 3 weeks to allow viral expression.

For pharmacological experiments, stainless steel internal guide cannulae (4 mm long, 26GA, Phymep) were bilaterally implanted in the aIC. Guide cannulae were cemented as described for fiber photometry implants at the following coordinates from Bregma in mm: 1.7 anterior, +/- 3.1 lateral and 2.5 ventral. After the cement dried, caps were screwed in the guide cannulae (small cap, Phymep).

For extracellular electrophysiological recordings, a 16-wire electrode array, arranged in a 4x4 grid (Innovative Neurophysiology) consisting of 35-µm tungsten wires with 150 µm spacing between wires, was implanted in the right aIC (coordinates from Bregma in mm: 1.7 anterior, +/- 3.1 lateral and 3.5 ventral). Additionally, electrodes were referenced via a silver ground placed above the right visual cortex. Recording electrodes were coated with red fluorescent tracer (DiI) before insertion into the brain. All implants were secured using Super-Bond cement (Sun Medical). After surgery, mice were allowed to recover for four days and were habituated to handling and headstage connection for 3 days.

Fig.	Coordinates AP/ML/DV (mm)	Viral vector	V(nL)	Titer (vg/mL)	Provider
1a-c	**aIC**: +1.7 / +3.1 / -3.5 **pIC**: -0.35 / +4.0 / -4.2	CTB AF-488 or AF-555 (counterbalanced)	250	-	Fisher Scientific 488: 11544267 555: 11554267
S1b-e S1h-l	**VTA**: -3.2 / +0.4 / -4.35 **SNc**: -3.16 / +1.5 / -4.2 **aIC**: +1.7 / +3.1 / -3.5 **pIC**: -0.35 / +4.0 / -4.2	AAV_9- EF1α-DIO-eYFP	400 250 250	$6.69.10^{13}$	Addgene 27056-AAV9
S1h-l	**aIC**: +1.7 / +3.1 / -3.5 **pIC**: -0.35 / +4.0 / -4.2	$AAV_{8/2}$-hEF1α -DIO-Synaptophysin-mCherry	250	$2.5.\ 10^{13}$	Massachusetts General Hospital AAV-RN1
2a-i S2a-f	**aIC**: +1.7 / +3.1 / -3.5 **pIC**: -0.35 / +4.0 / -4.2	AAV_1.hSyn.dLight1.1	250	$\geq 7.10^{12}$	Addgene 111066-AAV1
2j-u S2g-y	**aIC**: +1.7 / +3.1 / -3.5	AAV_9.hSyn.DIO.$GRAB_{DA3m}$	250	$\geq 2.10^{12}$	From Yulong Li Vector Builder
In vivo recordings	Red DiI used to coat electrodes before implantation				ThermoFisher V22885

Table 1. Details of coordinates, neuronal tracing and viral vectors.

Anatomical characterization of the dopaminergic system in IC. All images were acquired with a Leica SP8 confocal microscope (Leica Microscopy) and analyzed using ImageJ Software. To quantify the dopaminergic cell bodies in the VTA and SNc whose axons branch in the IC, we captured images with an area of 276,79 µm² and with a format of 1024x1024 pixels at 40X magnification. The regions of interest were selected using the Allen Brain Atlas, and brain sections had Bregma coordinates ranging from -2.80 mm to -3.52 mm. Cell bodies positively stained with either tracer CTB-488 or -555 and colocalized with tyrosine hydroxylase were considered as dopaminergic neurons. Similarly, to quantify axonal densities from VTA and SNc neurons targeting the insula labeled with eYFP fluorescence, we imaged the aIC and contralateral aIC (contra-aIC, Bregma: +1.70mm), pIC and contralateral pIC (contra-pIC, Bregma: -0.35mm). Picture format was set at 1024x1024 pixels (Number of z-stacks: 20, z-steps: ~ 1 ± 0.10 µm, 15 frames average) and for axonal quantification, z-stack images were processed altogether.

Fluorescent *in situ* hybridization (FISH). Staining for *Drd1* and *Drd2* mRNAs was performed using single molecule FISH (smFISH). Brains from four C57Bl/6J 8-week-old male mice were rapidly extracted and snap-frozen on dry ice and stored at −80 °C until use. Anterior and posterior insular cortex coronal sections (16 µm) were collected directly onto Superfrost Plus slides (Fisherbrand). RNAscope Fluorescent Multiplex labeling kit (ACDBio; Cat# 323110) was used to perform the smFISH assay according to the manufacturer's recommendations. Probes used for staining are mm-Drd1-C2 (ACDBio, Cat# 406491-C2), mm-Drd1-C1 (ACDBio, Cat# 461901), mm-Drd2-C3 (ACDBio, Cat# 406501-C3), mm-Slc17a7-C1 (ACDBio; Cat# 416631) and mm-Slc32a1-C2 (ACDBio, Cat# 319191-C2). After incubation with fluorescent-labeled probes, slides were counterstained with DAPI and mounted with ProLong Diamond Antifade mounting medium.

Behavioral assays. The temperature and humidity of the experiment room were controlled at 20 to 24°C and 45% to 65%, respectively. Animals were handled for 15 minutes, at least once a day, and habituated to being connected one week before the photometry and *in vivo* electrophysiology experiments. All tests were performed in the dark phase (active phase) of the reversed light/dark cycle. Behavioral mazes were always cleaned with acetic acid 2% and distilled water before each animal session. One camera on top of the experimental apparatus was used for all tests to track the animal's position and then synchronized with related activities.

Anxiety assays: we used two recognized tests with predictive validity: the elevated plus maze (EPM, Lister, 1987) and the open field test (OFT, Prut & Belzung, 2003). Elevated plus maze: The arena has a plus shape (75 x 75 cm) at 60 cm height, consisting of two open arms (anxiogenic spaces) and two closed arms (protected areas) of 5 cm width. Each animal was placed at the center and facing one open arm and left to explore it for 15 minutes. Open field test: the arena is squared (60 x 60 cm) and the anxiogenic space is the center, while the protected spaces are the borders of the field. The center is defined as 50% of the total open-field arena. Each animal was put in the open field and left to explore it for 20 minutes.

Innate valence assays: to assess taste valence, mice were food-deprived 20 hours prior to the sucrose/quinine test. An Arduino-controlled device was used to randomly deliver either 15 % sucrose (60% of trials, pseudorandom) or 1 mM quinine (40% of trials, pseudorandom) in the center of a 30 x 30 cm squared arena. Each tastant was delivered for 20 seconds and the inter-trial interval (ITI) was 10 seconds. Sucrose and quinine consumptions were measured using 2 LEDs that blinked each time the mouse licked the tastant. Mild foot shocks: 10 foot shocks (0.3 mA) of 1 second each were delivered every minute.

Fiber-photometry recordings. [1] Acquisition: dLight1.1 and $GRAB_{DA3m}$ photometry recordings were carried out using low-power blue excitation light (470 nm LED, 30-40 µW) at the tip of the patch cord via a 0.29 NA patch cords. The green light emitted by dLight1.1 and $GRAB_{DA3m}$ was collected through the same patch cord and routed via a 20x objective lens connected to a complementary metal-oxide semiconductor (CMOS). The isosbestic wavelength of 405 nm was used to remove motion-related artifacts and signals unrelated to neuronal activity since it is independent of DA concentration. dLight1.1 and $GRAB_{DA3m}$ emission light were bandpass filtered and focused on CMOS camera sensor for fluorescence detection. The sampling rate was set at 20 Hz for both photometry and video recordings. [2] Data analysis: photometry signals were processed and analyzed using custom-written Matlab scripts as described in Nicolas et al., 2023.

***In vivo* pharmacology.** [1] For bilateral intracranial infusion of the selective D1 agonist SKF38393 (Fig. 3), mice were handled for 5 days to habituate them to be restrained and to have connections to their guide cannulae. 33GA stainless steel internal canulae (5 mm long, Phymep) projecting 1 mm beyond the tip of the 26 GA guide cannula were connected to Hamilton syringe place into a pump (KDS legato 101, Phymep). Coordinates from Bregma of the tip of the internal cannulae in mm: 1.7 anterior, +/-3.1 lateral and 3.5 ventral. The D1 agonist SKF38393 hydrobromide (0.25 mg/mL, Tocris) was diluted in sterile saline (0.9% NaCl). To ensure good injections, the drug was diluted with 0.5% of CTB-AF555 0.4% (Fisher Scientific). Half of the mice received 250 nL in each hemisphere of the D1 agonist SKF38393 or the Vehicle (sterile saline) at a rate of 1 $\mu L.min^{-1}$. Internal cannulae were withdrawn 1 min after the end of the infusion, and after 5 additional minutes, mice were placed in the center of the EPM, facing an open arm for 15 minutes. [2] For intraperitoneal (i.p.) injection of the selective D1 agonist SKF38393 (Fig. 3), mice were habituated for 2 days to the i.p. injections. On the test day, mice received either an i.p. injection of sterile saline (0.9% NaCl) or the D1 agonist SKF38393 diluted with sterile saline (10 mg/kg). After 30 minutes post-injection, mice were placed in the EPM for 15 minutes.

***In vivo* electrophysiology**

Single-unit recordings. 16-channel electrodes were attached to an 18-pin nanoconnector (Omnetics A79014-001) and connected to a headstage containing 16 unity-gain operational amplifiers (Intan, RHD2132). Extracellular single units were recorded via the Open Ephys

acquisition board (Open Ephys, Siegle et al., 2017) at 30 kHz with high-pass and low-pass filter cut-offs of 300 Hz to 6 kHz, respectively, and synchronized with behavior.

Spike sorting. Single-unit action potentials were isolated and analyzed using custom Python scripts. Spike detection and sorting were performed with the semi-automatic spike sorter Kilosort 4 (Pachitariu et al., 2024). The common reference electrode was removed along with channel-by-channel normalization. Principal component analysis was done per channel on the 16 channels. A group of action potential waveforms was generated from a single neuron if the waveforms formed a discrete, isolated cluster in the principal-component space and had a refractory period longer than 1 ms. Quality controls include observing cluster and ratio similarities to ensure proper segregation of multi-unit into single-unit activity.

Extracting behavior. Mouse position in the EPM was tracked using DeepLabCut (version 2.3.6, Mathis et al., 2018; Nath et al., 2019). 20 frames from each 15-min video were annotated manually for the following body parts: snout, left and right ear, neck, backbone (3 points), tail base, tail middle and tail end. A residual network (resnet-50 model, He et al., 2015) was trained over 80% (100 000 iterations) of the manually annotated frames. To account for head dips, a threshold of tolerance was set to widen the EPM coordinates, which was defined as the average difference between the tracked snout and the shoulder of the mouse over time. All time points with tracked data outside the EPM were removed. Upon cleaning data and classifying the instantaneous positions within the EPM, the neural data for these corresponding time points were binned into 50 ms. Any head dip that happened within 1 second of the nearest previous head dip was not considered for analysis, hence we have a low number of head dips happening. Outliers were defined as any body part at a particular timepoint t that was more than 5 cm away from its previous position ($t-1$). The new position of that body part at time t was interpolated from the $t-10$ to $t+10$ points. This removes any erroneous and physically impossible coordinate locations generated by DLC.

Trial selection. Different behavioral events were defined such as: (1) entry to closed arm (CA entry), entry to open arm (OA entry) and head dip over the borders of EPM open arms (HD). Snippets of 6.5 seconds around the onset of these events were chosen. We then transformed the 25 ms-binned neural data into 250-ms bins with a 25-ms sliding time window to capture more robust and stable activity with neural snippets order as (units, time) in population vectors. Regarding taste valence experiments, 10-second neural snippets around the lick bout onsets were transformed into 250-ms data with a 25-ms sliding window.

Single-unit analysis. Neural snippets were trial-averaged and z-scored within a baseline period of [-3;-1] sec for the elevated-plus maze (Fig. 4) and [-5;-3] sec for the sucrose/quinine test (Fig. 5). We defined three classes of units based on their z-scored firing activity. For the elevated-plus maze, z-score > 1.65: excited units, z-score < -1.65: inhibited units, and -1.65 < z-score < 1.65: non-responding units. For sucrose/quinine test, z-score > 1.96: excited units, z-score < -1.65: inhibited units, and -1.65 < z-score < 1.96: non-responding units.

Population dynamics. Population vectors were trial-averaged per mouse and then z-scored. A global trial activity matrix containing the neural activity of all mice per trial type was constructed by concatenating trial-averaged population vectors of each trial-type along the time

dimension for each mouse. These concatenated activities per mouse were then joined along the unit axis. Principal component analysis (PCA) was performed on this global matrix. For statistical analysis, a leave-but-one approach (Li et al., 2022) was used. Each of the 11 mice was excluded from the global matrix and projected down to the same space as that of the PCA performed earlier. To be able to do this mathematically, units of each mouse to be excluded were deleted from the rows of the eigenvector matrix (n, n), where n is the total number of units for all mice) to get an ($n - n'$, n), where n' is the number of units in the said mouse. The all-but-one matrix was then projected onto this eigenvector space. We obtained 11 × 3 different reduced neural trajectories and quantified their relative trajectory lengths as the difference between the lengths of real and shuffled data (Data–Shuffle). As a control, the 15-minute neural data was shuffled across units, hence a spike was assigned to each timepoint based on a binomial distribution. These data were binned and analyzed the same way as the real data, and the same behavior was used to identify neural snippets corresponding to the different trial types.

Decoding trials. To assess the accuracy of neural data in decoding trial types, individual trial population vectors were z-scored and projected into the global PCA space. Decoding was performed using permutation testing, where a subset of trials was decoded across 100 iterations. To avoid any bias from a specific trial type or mouse, we ensured that the number of trials selected per trial type and mouse was uniform, based on one less than the minimum number of trials across all mice and trial types. A linear SVM was employed to decode these trials. The same procedure was applied to the shuffled data. Decoder performance was evaluated based on the accuracy of trial-type prediction:

$$\text{Accuracy} = \frac{\text{Trace(Confusion Matrix)}}{\text{sum(Trace(Confusion Matrix))}}$$

A confusion matrix represents the correct and incorrect predictions for each trial type. The diagonal of the matrix indicates the number of correctly predicted trials for each trial type. SVM decoding was performed at each time point, resulting in distribution of instantaneous decoding accuracies for both real and shuffled data.

Non-linear dimensionality reduction (CEBRA). To observe overall population dynamics on a continuous timescale, we used CEBRA (Consistent EmBeddings of high-dimensional Recordings using auxiliary, Schneider et al., 2023). We analyzed neural spike trains of 50-ms bins and used CEBRA Time, a self-supervised algorithm to do a discovery-driven analysis. We trained a pre-defined CEBRA model ('offset5' with the following parameters: learning rate = $3e^{-4}$, unit number in neural layers = 20, temperature = 1, iteration number = 40 000). Data was trained in a multi-session paradigm to remove the unwanted variance due to inherent small changes across animals and to discover robust latents that are invariant to animal. A control, comprising the shuffled data in a Poisson fashion, was also trained with the same multi-session paradigm. Decoding was performed when mice were located in the open and closed arms of the EPM. The decoding accurary was calculated using a k-Nearest Neighbor (kNN) classifier.

Population coding analysis. To decode neural correlates of anxiety in aIC, we quantified two variables from the neural latent embeddings: (1) the *Shannon entropy* as a measure of

uncertainty or randomness in a probability distribution. In the context of a neural latent embedding in the EPM and SQ, it will quantify the average level of "surprise" or unpredictability for the occurrence of a point within the latent space. Mathematically, Shannon entropy H is defined as:

$$H = -\sum_{i=0}^{k} p(x_i) \log_2 p(x_i)$$

where $p(x_i)$ represents the probability of occurrence of a specific point x_i in the latent embedding. Higher entropy indicates more uncertainty and a more uniform distribution of points, while lower entropy implies more predictability or concentration in the embedding space; (2) the distance between two barycenters (*barycenter distance*) in the latent embedding (open vs. closed arms and sucrose vs. quinine).

Brain extraction, histology, imaging. Animals were euthanized with pentobarbital (300 mg/kg) and perfused with ringer's solution followed by 4% PFA (antigenfix, F/P0014, MM France) at 4°C. Brains were extracted and left in 4% PFA overnight at 4°C for post fixation. Then, they were transferred to a 30% sucrose solution in PBS 1X at 4°C for cryoprotection. Then, the brains were embedded in optimum cutting temperature compound (OCT) and sliced into 100 or 50 µm coronal slices, with a freezing sliding microtome (12062999, Thermo Scientific). Sections were incubated with DAPI for 5 minutes, washed with PBS 1X twice for 5 minutes each, and then mounted on microscope slides with Polyvinyl alcohol PVA-DABCO mounting medium (Sigma Aldrich, France). All processed brain slices, as well as slices containing an injection site, were imaged using a 10X objective

Immunohistochemistry. To label dopaminergic neurons in VTA and SNc, 40-µm coronal slices between Bregma -2.80 mm and -3.52 mm were selected. Tissues were pre-treated with 3% Triton-X100 in PBS 1X, then blocked with 10% normal goat serum (NGS) and 3% Triton-X100 in PBS 1X for one hour at room temperature (RT) on a shaker. Tissues were transferred into primary antibody solution (Mouse anti-Tyrosine Hydroxylase, MAB318 from Millipore, 1:2000) in PBS with 3% Triton-100x and incubated overnight at 4°C. After three washing steps in 3%-Triton100x in PBS 1X, slices were incubated with a secondary antibody (Goat anti-mouse Alexa Fluor 647, A21236 from Fisher Scientific, 1:500) for two hours at RT. Tissues were rinsed three times with PBS 1X, transferred for 10 minutes in Hoechst solution (1:20000), and washed in PBS once.

Code availability. Custom-written codes used to analyze *in vivo* electrophysiology data are available upon request.

Statistical analysis. For statistical analyses, GraphPad Prism 10 was used. Normality and homogenous variance of the data were assessed by Shapiro-Wilk and F-test, respectively. We used two-tailed and paired/unpaired *t*-tests for single and paired comparisons. Multiple comparisons were assessed by one-way ANOVA followed by post-hoc Tukey's tests. For non-Normal

distributed data, Wilcoxon matched-pairs signed rank test was used for paired comparisons, and Friedman test followed by post-hoc Dunn's test was used for multiple comparisons. $p<0.05$ was considered statistically significant. For correlation analyses, Pearson's correlation coefficients (R^2) and linear regression were calculated.

Acknowledgments
We want to acknowledge the entire Beyeler Lab and past and present members, especially Débora Jacky and Anes Ju, for insightful discussions and advice. We thank Sara Laumond, Julie Tessaire, and the technical staff of the animal facility of the Neurocentre Magendie (INSERM 1215), especially Delphine Gonzales, Elizabeth Huc, Mégane Marion, and Jean-Baptiste Bernard, for their invaluable support. We thank the Bordeaux Imaging Center (BIC) for using their confocal microscope. We also thank Adeline Cathala and Luigi Bellocchio for their guidance and assistance with pharmacological experiments. We thank Sébastien Delcasso and Stéphane Valerio from Aquineuro for their support regarding *in vivo* electrophysiology experiments.

Funding
We gratefully acknowledge the support of the Région Nouvelle-Aquitaine, the INSERM 'ATIP/Avenir' program, the Fondation Schlumberger pour l'Education et la Recherche (FSER), the French National Research Agency (ANR, grants: 'CEA' and 'INSULA' to AB and ANR-20-CE14-0020 to EV), and the Fondation Bettencourt Schueller (Impulscience grant) provided to AB. This work was supported by Fondation pour la Recherche Médicale (EQU202203014705 to EV, "Equipes FRM" to AB, "Fin de thèse" grant (FDT202304016426) to YC and the "postdoctoral fellowship" to CN (ARF201909009147). We also acknowledge the FENS-Kavli Network for supporting YC's exchange in JG's lab.

Authorship contributions
YC and AB conceptualized the study. AB provided support for all experiments except those involving FISH. YC contributed to the analysis of all experiments.
Dopaminergic system anatomy in the insular cortex. MA conducted the anatomical mapping of D1-expressing insula neurons and GV the D2-expressing insula neurons. EV performed the FISH experiments, and DR analyzed the FISH data.
Photometry recordings of dopamine release. YC performed and analyzed the dLight1.1 recordings, YL provided the $GRAB_{DA3m}$ cre-dependent plasmid, and GV performed and analyzed the $GRAB_{DA3m}$ recordings.
Pharmacology. YC, GV, DR, CN, and TH conducted pharmacological experiments.
Single-unit recordings and analysis. YC performed *in vivo* single-unit recordings while TDR, AG, and DR assisted in analyzing this data. TDR and AG wrote computational analysis scripts for the study. YKW and JG provided help in the analysis.
Manuscript. YC and AB wrote the original draft of the manuscript. YC made all the figures. All authors critically reviewed and approved the final version before submission.

Competing interests

The authors declare that they do not have any competing interests or conflicts of interest (financial or otherwise) related to the material presented in this manuscript.

Bibliography

Alvarez, R. P., Kirlic, N., Misaki, M., Bodurka, J., Rhudy, J. L., Paulus, M. P., & Drevets, W. C. (2015). Increased anterior insula activity in anxious individuals is linked to diminished perceived control. *Translational Psychiatry*, *5*(6), e591–e591. https://doi.org/10.1038/tp.2015.84

Anastasiades, P. G., Boada, C., & Carter, A. G. (2019). Cell-Type-Specific D1 Dopamine Receptor Modulation of Projection Neurons and Interneurons in the Prefrontal Cortex. *Cerebral Cortex (New York, N.Y.: 1991)*, *29*(7), 3224–3242. https://doi.org/10.1093/cercor/bhy299

Bananej, M., Karimi-Sori, A., Zarrindast, M. R., & Ahmadi, S. (2012). D1 and D2 dopaminergic systems in the rat basolateral amygdala are involved in anxiogenic-like effects induced by histamine. *Journal of Psychopharmacology*, *26*(4), 564–574. https://doi.org/10.1177/0269881111405556

Belzung, C., & Griebel, G. (2001). Measuring normal and pathological anxiety-like behaviour in mice: A review. *Behavioural Brain Research*, *125*(1–2), 141–149. https://doi.org/10.1016/S0166-4328(01)00291-1

Beyeler, A., Namburi, P., Glober, G. F., Simonnet, C., Calhoon, G. G., Conyers, G. F., Luck, R., Wildes, C. P., & Tye, K. M. (2016). Divergent Routing of Positive and Negative Information from the Amygdala during Memory Retrieval. *Neuron*, *90*(2), 348–361. https://doi.org/10.1016/j.neuron.2016.03.004

Bittar, T. P., Pelaez, M. C., Silva, J. C. H., Quessy, F., Lavigne, A.-A., Morency, D., Blanchette, L.-J., Arsenault, E., Cherasse, Y., Seigneur, J., Timofeev, I., Sephton, C. F., Proulx, C. D., & Labonté, B. (2021). Chronic Stress Induces Sex-Specific Functional and Morphological Alterations in Corticoaccumbal and Corticotegmental Pathways. *Biological Psychiatry*, *90*(3), 194–205. https://doi.org/10.1016/j.biopsych.2021.02.014

Bordes, J., Miranda, L., Reinhardt, M., Narayan, S., Hartmann, J., Newman, E. L., Brix, L. M., van Doeselaar, L., Engelhardt, C., Dillmann, L., Mitra, S., Ressler, K. J., Pütz, B., Agakov, F., Müller-Myhsok, B., & Schmidt, M. V. (2023). Automatically annotated motion tracking identifies a distinct social behavioral profile following chronic social defeat stress. *Nature Communications*, *14*(1), 4319. https://doi.org/10.1038/s41467-023-40040-3

Bromberg-Martin, E. S., Matsumoto, M., & Hikosaka, O. (2010). Dopamine in motivational control: Rewarding, aversive, and alerting. *Neuron*, *68*(5), 815–834. https://doi.org/10.1016/j.neuron.2010.11.022

Bruce, R. A., Weber, M. A., Bova, A. S., Volkman, R. A., Jacobs, C. E., Sivakumar, K., Stutt, H. R., Kim, Y., Curtu, R., & Narayanan, N. S. (2024). Complementary opposing D2-MSNs and D1-MSNs dynamics during interval timing. *eLife*, *13*. https://doi.org/10.7554/eLife.96287.2

Chang, S., Fermani, F., Huang, L., Schneider, S., Mathis, M. W., Deussing, J. M., & Cai, N. (2024). *Molecular and neural mechanisms of behavioural integration in the extended-amygdala* (p. 2024.04.29.591588). bioRxiv. https://doi.org/10.1101/2024.04.29.591588

Chen, K., Kogan, J. F., & Fontanini, A. (2021). Spatially Distributed Representation of Taste Quality in the Gustatory Insular Cortex of Behaving Mice. *Current Biology: CB*, *31*(2), 247-256.e4. https://doi.org/10.1016/j.cub.2020.10.014

Churchland, M. M., Cunningham, J. P., Kaufman, M. T., Ryu, S. I., & Shenoy, K. V. (2010). Cortical preparatory activity: Representation of movement or first cog in a dynamical machine? *Neuron*, *68*(3), 387–400. https://doi.org/10.1016/j.neuron.2010.09.015

Couderc, Y., & Beyeler, A. (2023). How an anxious heart talks to the brain. *Nature*, *615*(7951), 217–218. https://doi.org/10.1038/d41586-023-00502-6

Cruz, B. F., Guiomar, G., Soares, S., Motiwala, A., Machens, C. K., & Paton, J. J. (2022). Action suppression reveals opponent parallel control via striatal circuits. *Nature*, *607*(7919), 521–526. https://doi.org/10.1038/s41586-022-04894-9

Cunningham, J. P., & Yu, B. M. (2014). Dimensionality reduction for large-scale neural recordings. *Nature Neuroscience*, *17*(11), 1500–1509. https://doi.org/10.1038/nn.3776

Daviu, N., Bruchas, M. R., Moghaddam, B., Sandi, C., & Beyeler, A. (2019). Neurobiological links between stress and anxiety. *Neurobiology of Stress*, *11*, 100191. https://doi.org/10.1016/j.ynstr.2019.100191

de la Mora, M. P., Gallegos-Cari, A., Arizmendi-García, Y., Marcellino, D., & Fuxe, K. (2010). Role of dopamine receptor mechanisms in the amygdaloid modulation of fear and anxiety: Structural and functional analysis. *Progress in Neurobiology*, *90*(2), 198–216. https://doi.org/10.1016/j.pneurobio.2009.10.010

DeGroot, S. R., Zhao-Shea, R., Chung, L., Klenowski, P. M., Sun, F., Molas, S., Gardner, P. D., Li, Y., & Tapper, A. R. (2020). Midbrain Dopamine Controls Anxiety-like Behavior by Engaging Unique Interpeduncular Nucleus Microcircuitry. *Biological Psychiatry*, *88*(11), 855–866. https://doi.org/10.1016/j.biopsych.2020.06.018

Espinosa, P., Girard, B., Lucchini, M., Campanelli, F., Tiriticco, V., Mohrhauer, L., & Bellone, C. (2024). *Valence-dependent synaptic plasticity drives approach and avoidance behavior in social context* (p. 2022.11.08.515650). bioRxiv. https://doi.org/10.1101/2022.11.08.515650

Etkin, A., & Wager, T. D. (2007). Functional Neuroimaging of Anxiety: A Meta-Analysis of Emotional Processing in PTSD, Social Anxiety Disorder, and Specific Phobia. *American Journal of Psychiatry*, *164*(10), 1476–1488. https://doi.org/10.1176/appi.ajp.2007.07030504

Fallon, J. H. (1981). Collateralization of monoamine neurons: Mesotelencephalic dopamine projections to caudate, septum, and frontal cortex. *The Journal of Neuroscience: The Official Journal of the Society for Neuroscience*, *1*(12), Article 12. https://doi.org/10.1523/JNEUROSCI.01-12-01361.1981

Felix-Ortiz, A. C., Beyeler, A., Seo, C., Leppla, C. A., Wildes, C. P., & Tye, K. M. (2013). BLA to vHPC inputs modulate anxiety-related behaviors. *Neuron*, *79*(4), 658–664. https://doi.org/10.1016/j.neuron.2013.06.016

Gaspar, P., Bloch, B., & Le Moine, C. (1995). D1 and D2 Receptor Gene Expression in the Rat Frontal Cortex: Cellular Localization in Different Classes of Efferent Neurons. *European Journal of Neuroscience*, *7*(5), 1050–1063. https://doi.org/10.1111/j.1460-9568.1995.tb01092.x

Gehrlach, D. A., Dolensek, N., Klein, A. S., Roy Chowdhury, R., Matthys, A., Junghänel, M., Gaitanos, T. N., Podgornik, A., Black, T. D., Reddy Vaka, N., Conzelmann, K.-K., & Gogolla, N. (2019). Aversive state processing in the posterior insular cortex. *Nature Neuroscience*, *22*(9), Article 9. https://doi.org/10.1038/s41593-019-0469-1

Gehrlach, D. A., Weiand, C., Gaitanos, T. N., Cho, E., Klein, A. S., Hennrich, A. A., Conzelmann, K.-K., & Gogolla, N. (2020). A whole-brain connectivity map of mouse insular cortex. *eLife*, *9*, e55585. https://doi.org/10.7554/eLife.55585

Gerfen, C. R., Engber, T. M., Mahan, L. C., Susel, Z., Chase, T. N., Monsma, F. J., & Sibley, D. R. (1990). D1 and D2 Dopamine Receptor-regulated Gene Expression of Striatonigral and Striatopallidal Neurons. *Science*, *250*(4986), 1429–1432. https://doi.org/10.1126/science.2147780

Gil-Lievana, E., Ramírez-Mejía, G., Urrego-Morales, O., Luis-Islas, J., Gutierrez, R., & Bermúdez-Rattoni, F. (2022). Photostimulation of Ventral Tegmental Area-Insular Cortex Dopaminergic Inputs Enhances the Salience to Consolidate Aversive Taste Recognition Memory via D1-Like Receptors. *Frontiers in Cellular Neuroscience*, *16*. https://www.frontiersin.org/articles/10.3389/fncel.2022.823220

Glangetas, C., Guillaumin, A., Ladevèze, E., Braine, A., Gauthier, M., Bonamy, L., Doudnikoff, E., Dhellemmes, T., Landry, M., Bézard, E., Caille, S., Taupignon, A., Baufreton, J., & Georges, F. (2024). A population of Insula neurons encodes for social preference only after acute social isolation in mice. *Nature Communications*, *15*(1), 7142. https://doi.org/10.1038/s41467-024-51389-4

Godino, A., Salery, M., Minier-Toribio, A. M., Patel, V., Fullard, J. F., Parise, E. M., Martinez-Rivera, F. J., Morel, C., Roussos, P., Blitzer, R. D., & Nestler, E. J. (2023). *Dopaminoceptive D1 and D2 neurons in ventral hippocampus arbitrate approach and avoidance in anxiety* (p. 2023.07.25.550554). bioRxiv. https://doi.org/10.1101/2023.07.25.550554

Hare, B. D., & Duman, R. S. (2020). Prefrontal cortex circuits in depression and anxiety: Contribution of discrete neuronal populations and target regions. *Molecular Psychiatry*, *25*(11), Article 11. https://doi.org/10.1038/s41380-020-0685-9

Hare, B. D., Shinohara, R., Liu, R. J., Pothula, S., DiLeone, R. J., & Duman, R. S. (2019). Optogenetic stimulation of medial prefrontal cortex Drd1 neurons produces rapid and long-lasting antidepressant effects. *Nature Communications*, *10*(1), 223. https://doi.org/10.1038/s41467-018-08168-9

Hayden, E. P., Klein, D. N., Dougherty, L. R., Olino, T. M., Laptook, R. S., Dyson, M. W., Bufferd, S. J., Durbin, C. E., Sheikh, H. I., & Singh, S. M. (2010). The dopamine D2 receptor gene and depressive and anxious symptoms in childhood: Associations and evidence for gene–environment correlation and gene–environment interaction. *Psychiatric Genetics*, *20*(6), Article 6. https://doi.org/10.1097/YPG.0b013e32833adccb

He, K., Zhang, X., Ren, S., & Sun, J. (2015). *Deep Residual Learning for Image Recognition* (arXiv:1512.03385). arXiv. https://doi.org/10.48550/arXiv.1512.03385

Herring, C. A., Simmons, R. K., Freytag, S., Poppe, D., Moffet, J. J. D., Pflueger, J., Buckberry, S., Vargas-Landin, D. B., Clément, O., Echeverría, E. G., Sutton, G. J., Alvarez-Franco, A., Hou, R., Pflueger, C., McDonald, K., Polo, J. M., Forrest, A. R. R., Nowak, A. K., Voineagu, I., … Lister, R. (2022). Human prefrontal cortex

gene regulatory dynamics from gestation to adulthood at single-cell resolution. *Cell*, *185*(23), 4428-4447.e28. https://doi.org/10.1016/j.cell.2022.09.039

Hjorth, O. R., Frick, A., Gingnell, M., Hoppe, J. M., Faria, V., Hultberg, S., Alaie, I., Månsson, K. N. T., Rosén, J., Reis, M., Wahlstedt, K., Jonasson, M., Lubberink, M., Antoni, G., Fredrikson, M., & Furmark, T. (2021). Expectancy effects on serotonin and dopamine transporters during SSRI treatment of social anxiety disorder: A randomized clinical trial. *Translational Psychiatry*, *11*(1), Article 1. https://doi.org/10.1038/s41398-021-01682-3

Hsueh, B., Chen, R., Jo, Y., Tang, D., Raffiee, M., Kim, Y. S., Inoue, M., Randles, S., Ramakrishnan, C., Patel, S., Kim, D. K., Liu, T. X., Kim, S. H., Tan, L., Mortazavi, L., Cordero, A., Shi, J., Zhao, M., Ho, T. T., … Deisseroth, K. (2023). Cardiogenic control of affective behavioural state. *Nature*, *615*(7951), Article 7951. https://doi.org/10.1038/s41586-023-05748-8

Hurd, Y. L., Suzuki, M., & Sedvall, G. C. (2001). D1 and D2 dopamine receptor mRNA expression in whole hemisphere sections of the human brain. *Journal of Chemical Neuroanatomy*, *22*(1–2), 127–137. https://doi.org/10.1016/s0891-0618(01)00122-3

Jenni, N. L., Larkin, J. D., & Floresco, S. B. (2017). Prefrontal dopamine D1 and D2 receptors regulate dissociable aspects of decision-making via distinct ventral striatal and amygdalar circuits. *Journal of Neuroscience*. https://doi.org/10.1523/JNEUROSCI.0030-17.2017

Jimenez, J. C., Su, K., Goldberg, A. R., Luna, V. M., Biane, J. S., Ordek, G., Zhou, P., Ong, S. K., Wright, M. A., Zweifel, L., Paninski, L., Hen, R., & Kheirbek, M. A. (2018). Anxiety Cells in a Hippocampal-Hypothalamic Circuit. *Neuron*, *97*(3), 670-683.e6. https://doi.org/10.1016/j.neuron.2018.01.016

Kim, H. R., Malik, A. N., Mikhael, J. G., Bech, P., Tsutsui-Kimura, I., Sun, F., Zhang, Y., Li, Y., Watabe-Uchida, M., Gershman, S. J., & Uchida, N. (2020). A Unified Framework for Dopamine Signals across Timescales. *Cell*, *183*(6), 1600-1616.e25. https://doi.org/10.1016/j.cell.2020.11.013

Klumpp, H., Fitzgerald, D. A., & Phan, K. L. (2013). Neural predictors and mechanisms of cognitive behavioral therapy on threat processing in social anxiety disorder. *Progress in Neuro-Psychopharmacology & Biological Psychiatry*, *45*, 83–91. https://doi.org/10.1016/j.pnpbp.2013.05.004

Krok, A. C., Maltese, M., Mistry, P., Miao, X., Li, Y., & Tritsch, N. X. (2023). Intrinsic dopamine and acetylcholine dynamics in the striatum of mice. *Nature*, *621*(7979), 543–549. https://doi.org/10.1038/s41586-023-05995-9

Kusumoto-Yoshida, I., Liu, H., Chen, B. T., Fontanini, A., & Bonci, A. (2015). Central role for the insular cortex in mediating conditioned responses to anticipatory cues. *Proceedings of the National Academy of Sciences*, *112*(4), 1190–1195. https://doi.org/10.1073/pnas.1416573112

Lammel, S., Lim, B. K., & Malenka, R. C. (2014). Reward and aversion in a heterogeneous midbrain dopamine system. *Neuropharmacology*, *76 Pt B*(0 0), 351–359. https://doi.org/10.1016/j.neuropharm.2013.03.019

LeDuke, D. O., Borio, M., Miranda, R., & Tye, K. M. (2023). Anxiety and depression: A top-down, bottom-up model of circuit function. *Annals of the New York Academy of Sciences*, *1525*(1), 70–87. https://doi.org/10.1111/nyas.14997

Li, H., Namburi, P., Olson, J. M., Borio, M., Lemieux, M. E., Beyeler, A., Calhoon, G. G., Hitora-Imamura, N., Coley, A. A., Libster, A., Bal, A., Jin, X., Wang, H., Jia, C., Choudhury, S. R., Shi, X., Felix-Ortiz, A. C., de la Fuente, V., Barth, V. P., … Tye, K. M. (2022). Neurotensin orchestrates valence assignment in the amygdala. *Nature*, *608*(7923), 586–592. https://doi.org/10.1038/s41586-022-04964-y

Lister, RichardG. (1987). The use of a plus-maze to measure anxiety in the mouse. *Psychopharmacology*, *92*(2). https://doi.org/10.1007/BF00177912

Livneh, Y., Sugden, A. U., Madara, J. C., Essner, R. A., Flores, V. I., Sugden, L. A., Resch, J. M., Lowell, B. B., & Andermann, M. L. (2020). Estimation of Current and Future Physiological States in Insular Cortex. *Neuron*, *105*(6), 1094-1111.e10. https://doi.org/10.1016/j.neuron.2019.12.027

Lüthi, A., & Lüscher, C. (2014). Pathological circuit function underlying addiction and anxiety disorders. *Nature Neuroscience*, *17*(12), 1635–1643. https://doi.org/10.1038/nn.3849

MacLeod, C., Grafton, B., & Notebaert, L. (2019). Anxiety-Linked Attentional Bias: Is It Reliable? *Annual Review of Clinical Psychology*, *15*(Volume 15, 2019), 529–554. https://doi.org/10.1146/annurev-clinpsy-050718-095505

Martel, J. C., & Gatti McArthur, S. (2020). Dopamine Receptor Subtypes, Physiology and Pharmacology: New Ligands and Concepts in Schizophrenia. *Frontiers in Pharmacology*, *11*. https://www.frontiersin.org/articles/10.3389/fphar.2020.01003

Mathis, A., Mamidanna, P., Cury, K. M., Abe, T., Murthy, V. N., Mathis, M. W., & Bethge, M. (2018). DeepLabCut: Markerless pose estimation of user-defined body parts with deep learning. *Nature Neuroscience*, *21*(9), 1281–1289. https://doi.org/10.1038/s41593-018-0209-y

Mathis, M. W., Rotondo, A. P., Chang, E. F., Tolias, A. S., & Mathis, A. (2024). Decoding the brain: From neural representations to mechanistic models. *Cell*, *187*(21), 5814–5832. https://doi.org/10.1016/j.cell.2024.08.051

Meador-Woodruff, J. H., Damask, S. P., Wang, J., Haroutunian, V., Davis, K. L., & Watson, S. J. (1996). Dopamine Receptor mRNA Expression in Human Striatum and Neocortex. *Neuropsychopharmacology*, *15*(1), 17–29. https://doi.org/10.1016/0893-133X(95)00150-C

Méndez-Ruette, M., Linsambarth, S., Moraga-Amaro, R., Quintana-Donoso, D., Méndez, L., Tamburini, G., Cornejo, F., Torres, R. F., & Stehberg, J. (2019). The Role of the Rodent Insula in Anxiety. *Frontiers in Physiology*, *10*. https://www.frontiersin.org/articles/10.3389/fphys.2019.00330

Mizuhiki, T., Richmond, B. J., & Shidara, M. (2007). Mode changes in activity of single neurons in anterior insular cortex across trials during multi-trial reward schedules. *Neuroscience Research*, *57*(4), 587–591. https://doi.org/10.1016/j.neures.2006.12.008

Molas, S., Zhao-Shea, R., Freels, T. G., & Tapper, A. R. (2023). Viral Tracing Confirms Paranigral Ventral Tegmental Area Dopaminergic Inputs to the Interpeduncular Nucleus Where Dopamine Release Encodes Motivated Exploration. *eNeuro*, *10*(1). https://doi.org/10.1523/ENEURO.0282-22.2022

Morel, C., Montgomery, S. E., Li, L., Durand-de Cuttoli, R., Teichman, E. M., Juarez, B., Tzavaras, N., Ku, S. M., Flanigan, M. E., Cai, M., Walsh, J. J., Russo, S. J., Nestler, E. J., Calipari, E. S., Friedman, A. K., & Han, M.-H. (2022). Midbrain projection to the basolateral amygdala encodes anxiety-like but not depression-like behaviors. *Nature Communications*, *13*(1), Article 1. https://doi.org/10.1038/s41467-022-29155-1

Nath, T., Mathis, A., Chen, A. C., Patel, A., Bethge, M., & Mathis, M. W. (2019). Using DeepLabCut for 3D markerless pose estimation across species and behaviors. *Nature Protocols*, *14*(7), 2152–2176. https://doi.org/10.1038/s41596-019-0176-0

Nicolas, C., Ju, A., Wu, Y., Eldirdiri, H., Delcasso, S., Couderc, Y., Fornari, C., Mitra, A., Supiot, L., Vérité, A., Masson, M., Rodriguez-Rozada, S., Jacky, D., Wiegert, J. S., & Beyeler, A. (2023). Linking emotional valence and anxiety in a mouse insula-amygdala circuit. *Nature Communications*, *14*(1), Article 1. https://doi.org/10.1038/s41467-023-40517-1

Nicolas, C., Russell, T. I., Pierce, A. F., Maldera, S., Holley, A., You, Z.-B., McCarthy, M. M., Shaham, Y., & Ikemoto, S. (2019). Incubation of Cocaine Craving After Intermittent-Access Self-administration: Sex Differences and Estrous Cycle. *Biological Psychiatry*, *85*(11), 915–924. https://doi.org/10.1016/j.biopsych.2019.01.015

Ohara, P. T., Granato, A., Moallem, T. M., Wang, B.-R., Tillet, Y., & Jasmin, L. (2003). Dopaminergic input to GABAergic neurons in the rostral agranular insular cortex of the rat. *Journal of Neurocytology*, *32*(2), Article 2. https://doi.org/10.1023/b:neur.0000005598.09647.7f

Pachitariu, M., Sridhar, S., Pennington, J., & Stringer, C. (2024). Spike sorting with Kilosort4. *Nature Methods*, *21*(5), 914–921. https://doi.org/10.1038/s41592-024-02232-7

Pang, R., Lansdell, B. J., & Fairhall, A. L. (2016). Dimensionality reduction in neuroscience. *Current Biology*, *26*(14), R656–R660. https://doi.org/10.1016/j.cub.2016.05.029

Park, S., Cho, J., & Huh, Y. (2022). Role of the anterior insular cortex in restraint-stress induced fear behaviors. *Scientific Reports*, *12*(1), 6504. https://doi.org/10.1038/s41598-022-10345-2

Patriarchi, T., Cho, J. R., Merten, K., Howe, M. W., Marley, A., Xiong, W.-H., Folk, R. W., Broussard, G. J., Liang, R., Jang, M. J., Zhong, H., Dombeck, D., von Zastrow, M., Nimmerjahn, A., Gradinaru, V., Williams, J. T., & Tian, L. (2018). Ultrafast neuronal imaging of dopamine dynamics with designed genetically encoded sensors. *Science*, *360*(6396), eaat4422. https://doi.org/10.1126/science.aat4422

Paulus, M. P., & Stein, M. B. (2006). An insular view of anxiety. *Biological Psychiatry*, *60*(4), 383–387. https://doi.org/10.1016/j.biopsych.2006.03.042

Peng, Y., Gillis-Smith, S., Jin, H., Tränkner, D., Ryba, N. J. P., & Zuker, C. S. (2015). Sweet and bitter taste in the brain of awake behaving animals. *Nature*, *527*(7579), Article 7579. https://doi.org/10.1038/nature15763

Pignatelli, M., & Beyeler, A. (2019). Valence coding in amygdala circuits. *Current Opinion in Behavioral Sciences*, *26*, 97–106. https://doi.org/10.1016/j.cobeha.2018.10.010

Prut, L., & Belzung, C. (2003). The open field as a paradigm to measure the effects of drugs on anxiety-like behaviors: A review. *European Journal of Pharmacology*, *463*(1), 3–33. https://doi.org/10.1016/S0014-2999(03)01272-X

Puig, M. V., & Miller, E. K. (2012). The Role of Prefrontal Dopamine D1 Receptors in the Neural Mechanisms of Associative Learning. *Neuron*, *74*(5), 10.1016/j.neuron.2012.04.018. https://doi.org/10.1016/j.neuron.2012.04.018

Qi, G., Zhang, P., Li, T., Li, M., Zhang, Q., He, F., Zhang, L., Cai, H., Lv, X., Qiao, H., Chen, X., Ming, J., & Tian, B. (2022). NAc-VTA circuit underlies emotional stress-induced anxiety-like behavior in the three-chamber vicarious social defeat stress mouse model. *Nature Communications*, *13*(1), Article 1. https://doi.org/10.1038/s41467-022-28190-2

Sala-Bayo, J., Fiddian, L., Nilsson, S. R. O., Hervig, M. E., McKenzie, C., Mareschi, A., Boulos, M., Zhukovsky, P., Nicholson, J., Dalley, J. W., Alsiö, J., & Robbins, T. W. (2020). Dorsal and ventral striatal dopamine D1 and D2 receptors differentially modulate distinct phases of serial visual reversal learning. *Neuropsychopharmacology*, *45*(5), 736–744. https://doi.org/10.1038/s41386-020-0612-4

Schneider, S., Lee, J. H., & Mathis, M. W. (2023). Learnable latent embeddings for joint behavioural and neural analysis. *Nature*, *617*(7960), Article 7960. https://doi.org/10.1038/s41586-023-06031-6

Shah, S. G., Klumpp, H., Angstadt, M., Nathan, P. J., & Phan, K. L. (2009). Amygdala and insula response to emotional images in patients with generalized social anxiety disorder. *Journal of Psychiatry & Neuroscience : JPN*, *34*(4), 296–302.

Siegle, J. H., López, A. C., Patel, Y. A., Abramov, K., Ohayon, S., & Voigts, J. (2017). Open Ephys: An open-source, plugin-based platform for multichannel electrophysiology. *Journal of Neural Engineering*, *14*(4), 045003. https://doi.org/10.1088/1741-2552/aa5eea

Siju, K. P., Štih, V., Aimon, S., Gjorgjieva, J., Portugues, R., & Grunwald Kadow, I. C. (2020). Valence and State-Dependent Population Coding in Dopaminergic Neurons in the Fly Mushroom Body. *Current Biology*, *30*(11), 2104-2115.e4. https://doi.org/10.1016/j.cub.2020.04.037

Sippy, T., & Tritsch, N. X. (2023). Unraveling the dynamics of dopamine release and its actions on target cells. *Trends in Neurosciences*, *46*(3), 228–239. https://doi.org/10.1016/j.tins.2022.12.005

Sun, F., Zhou, J., Dai, B., Qian, T., Zeng, J., Li, X., Zhuo, Y., Zhang, Y., Wang, Y., Qian, C., Tan, K., Feng, J., Dong, H., Lin, D., Cui, G., & Li, Y. (2020). Next-generation GRAB sensors for monitoring dopaminergic activity in vivo. *Nature Methods*, *17*(11), 1156–1166. https://doi.org/10.1038/s41592-020-00981-9

Tong, Q., Cui, X., Xu, H., Zhang, X., Hu, S., Huang, F., & Xiao, L. (2023). D1 receptor-expressing neurons in ventral tegmental area alleviate mouse anxiety-like behaviors via glutamatergic projection to lateral septum. *Molecular Psychiatry*, *28*(2), Article 2. https://doi.org/10.1038/s41380-022-01809-y

Tovote, P., Fadok, J. P., & Lüthi, A. (2015). Neuronal circuits for fear and anxiety. *Nature Reviews Neuroscience*, *16*(6), 317–331. https://doi.org/10.1038/nrn3945

Tritsch, N. X., & Sabatini, B. L. (2012). Dopaminergic modulation of synaptic transmission in cortex and striatum. *Neuron*, *76*(1), 33–50. https://doi.org/10.1016/j.neuron.2012.09.023

Vander Weele, C. M., Siciliano, C. A., Matthews, G. A., Namburi, P., Izadmehr, E. M., Espinel, I. C., Nieh, E. H., Schut, E. H. S., Padilla-Coreano, N., Burgos-Robles, A., Chang, C.-J., Kimchi, E. Y., Beyeler, A., Wichmann, R., Wildes, C. P., & Tye, K. M. (2018). Dopamine enhances signal-to-noise ratio in cortical-brainstem encoding of aversive stimuli. *Nature*, *563*(7731), Article 7731. https://doi.org/10.1038/s41586-018-0682-1

Vincis, R., Chen, K., Czarnecki, L., Chen, J., & Fontanini, A. (2020). Dynamic Representation of Taste-Related Decisions in the Gustatory Insular Cortex of Mice. *Current Biology*, *30*(10), 1834-1844.e5. https://doi.org/10.1016/j.cub.2020.03.012

Watabe-Uchida, M., Eshel, N., & Uchida, N. (2017). Neural Circuitry of Reward Prediction Error. *Annual Review of Neuroscience*, *40*, 373–394. https://doi.org/10.1146/annurev-neuro-072116-031109

Weger, M., & Sandi, C. (2018). High anxiety trait: A vulnerable phenotype for stress-induced depression. *Neuroscience & Biobehavioral Reviews*, *87*, 27–37. https://doi.org/10.1016/j.neubiorev.2018.01.012

Wu, Q.-F., Yang, L., Li, S., Wang, Q., Yuan, X.-B., Gao, X., Bao, L., & Zhang, X. (2012). Fibroblast Growth Factor 13 Is a Microtubule-Stabilizing Protein Regulating Neuronal Polarization and Migration. *Cell*, *149*(7), 1549–1564. https://doi.org/10.1016/j.cell.2012.04.046

Xing, B., Mack, N. R., Zhang, Y.-X., McEachern, E. P., & Gao, W.-J. (2022). Distinct Roles for Prefrontal Dopamine D1 and D2 Neurons in Social Hierarchy. *Journal of Neuroscience*, *42*(2), 313–324. https://doi.org/10.1523/JNEUROSCI.0741-21.2021

Zalachoras, I., Astori, S., Meijer, M., Grosse, J., Zanoletti, O., de Suduiraut, I. G., Deussing, J. M., & Sandi, C. (2022). Opposite effects of stress on effortful motivation in high and low anxiety are mediated by CRHR1 in the VTA. *Science Advances*, *8*(12), eabj9019. https://doi.org/10.1126/sciadv.abj9019

Zarrindast, M.-R., & Khakpai, F. (2015). The Modulatory Role of Dopamine in Anxiety-like Behavior. *Archives of Iranian Medicine*, *18*(9), 591–603.

Zhuo, Y., Luo, B., Yi, X., Dong, H., Miao, X., Wan, J., Williams, J. T., Campbell, M. G., Cai, R., Qian, T., Li, F., Weber, S. J., Wang, L., Li, B., Wei, Y., Li, G., Wang, H., Zheng, Y., Zhao, Y., … Li, Y. (2024). Improved green and red GRAB sensors for monitoring dopaminergic activity in vivo. *Nature Methods*, *21*(4), 680–691. https://doi.org/10.1038/s41592-023-02100-w

Zweifel, L. S., Fadok, J. P., Argilli, E., Garelick, M. G., Jones, G. L., Dickerson, T. M. K., Allen, J. M., Mizumori, S. J. Y., Bonci, A., & Palmiter, R. D. (2011). Activation of dopamine neurons is critical for aversive conditioning and prevention of generalized anxiety. *Nature Neuroscience*, *14*(5), Article 5. https://doi.org/10.1038/nn.2808